

On the Effect of Aleatoric and Epistemic Errors on the Learnability and Quality of NN-based Potential Energy Surfaces

Sugata Goswami,^{†,§} Silvan Käser,[†] Raymond J. Bemish,[‡] and Markus Meuwly^{*,¶}

[†]*Department of Chemistry, University of Basel, Klingelbergstrasse 80, CH-4056 Basel,
Switzerland*

[‡]*Air Force Research Laboratory, Space Vehicles Directorate, Kirtland AFB, New Mexico
87117, USA*

[¶]*Department of Chemistry, University of Basel,
Klingelbergstrasse 80, 4056 Basel, Switzerland*

[§]*Present address: Department of Chemistry, Medi-Caps University, A.B. Road, Pigdamber,
Indore - 453 331 (M.P.), India*

E-mail: m.meuwly@unibas.ch

September 12, 2023

Abstract

The effect of noise in the input data for learning potential energy surfaces (PESs) based on neural networks for chemical applications is assessed. Noise in energies and forces can result from aleatoric and epistemic errors in the quantum chemical reference calculations. Statistical (aleatoric) noise arises for example due to the need to set convergence thresholds in the self consistent field (SCF) iterations whereas systematic (epistemic) noise is due to, *inter alia*, particular choices of basis sets in the calculations. The two molecules considered here as proxies are H₂CO and HONO which are examples for single- and multi-reference problems, respectively, for geometries around the minimum energy structure. For H₂CO it is found that adding noise to energies with magnitudes representative of single-point calculations does not deteriorate the quality of the final PESs whereas increasing the noise level commensurate with electronic structure calculations for more complicated, e.g. metal-containing, systems is expected to have a more notable effect. However, the effect of noise on the forces is more noticeable. On the other hand, for HONO which requires a multi-reference treatment, a clear correlation between model quality and the degree of multi-reference character as measured by the T_1 amplitude is found. It is concluded that for chemically "simple" cases the effect of aleatoric and epistemic noise is manageable without evident deterioration of the trained model - although the quality of the forces is important. However, considerably more care needs to be exercised for situations in which multi-reference effects are present.

1 Introduction

Machine learning (ML) has been established as a promising tool for representing inter- and intramolecular potential energy surfaces (PES) for applications in chemistry, physics, and

biophysics.¹⁻³ The great interest in developing and using such statistical models⁴ stems from the fact that - computationally expensive - energies (and forces) from electronic structure calculations can now be obtained at high levels of theory for large numbers of geometries whereas evaluation times for energies and forces of trained statistical models are comparatively short. As an example, for tri- and tetra-atomic molecules energies for $\sim 10^4$ geometries at the multi reference configuration interaction (MRCI) or coupled cluster singles doubles and perturbative triples (CCSD(T)) levels of theory can be determined routinely using at least aug-cc-pVTZ basis set quality.^{5,6} For larger molecules, containing up to 10 heavy atoms, energies based on MP2 or density functional theory (DFT) calculations using slightly smaller basis sets for $\sim 10^5$ geometries are routinely affordable.^{7,8}

An important aspect in the numerical treatment of chemical systems is the role played by inaccuracies inherent to such an approach. Every computational treatment has only finite accuracy and managing this aspect is important. The role of "noise" in machine-learned models has been considered from a number of perspectives. For one, it has been proposed to adapt the cost function to be minimized to account for errors in the input data.⁹ The cost function employed determines the noise-sensitivity of the model and is therefore a meaningful way to account for uncertainty on the input data. An alternative is to explicitly model the noise as an additional layer in the NN-architecture.¹⁰ Related to this, noise was included directly into the training ("training-with-noise algorithm"). Within this framework it was found that injecting measured amounts of noise of a particular structure can even improve the generalization capabilities for classification tasks.^{11,12} Finally, from the perspective of the type of uncertainty, aleatoric (statistical) and epistemic (systematic) uncertainties for the output of a trained NN have been analyzed for function estimation and classification.¹³

In the present work the role of noise in the input data is studied and analyzed for training multi-dimensional PESs based on reference *ab initio* calculations. Electronic structure cal-

culations in general require certain input from the user that controls the level of convergence of a calculation for a given conformation. For one, the self consistent field (SCF) calculation needs to be converged according to one or several properties, including the root mean squared (RMS) or the maximum change in the density matrix. This limits the aleatoric uncertainty of a calculation but does not influence the epistemic uncertainty. Hence, depending on the thresholds chosen at this step the final energy and associated forces for a given structure differ. This variability in the total energy induced, e.g., by particular choices of user-defined parameters is referred to as noise in the present work.

Depending on how complicated the electronic structure of a molecule is, more or less strict convergence criteria can be applied to the wavefunction at the SCF level. For closed-shell, single-reference species the tightest criteria possible are usually used whereas molecules containing transition metals can pose severe problems in terms of converging the reference wavefunction for a given geometry. Additional measures, such as “level shifting”¹⁴ may be required to converge energies for individual or even all conformations of interest. Again, this limits aleatoric but not epistemic uncertainty. Hence, determining the reference dataset for a full-dimensional, reactive PES for a species with complicated electronic structure can become a daunting task whereby individual geometries require dedicated adjustments of system parameters. This leads to variable aleatoric uncertainty across the reference data which is propagated into the model building and further influences the epistemic uncertainty of the final statistical model. Epistemic uncertainty arises due to the need to choose a particular basis set or to select a specific quantum chemical method which is an approximation to a full configuration interaction (FCI) treatment.

Such aspects become even more relevant when PESs are used in broader dynamics studies of chemical reactions. Using noisy reference data to represent the PES either as a neural network (NN) or with kernel-based methods, can lead to difficulties in training the statis-

tical model. It has, for example, been found that using reproducing kernel Hilbert space (RKHS) representations on electronic structure calculations for He-H₂⁺ at the full CI level work very reliably whereas for the same grid with energies determined from MRCI+Q calculations regularization is needed for a smooth representation.¹⁵ Hence, depending on the underlying quantum chemical method used the learnability differs and the resulting model is of higher or inferior quality. Such uncertainty will propagate through the entire pipeline which, in that case, consisted of running dynamics simulations on the PES and determining observables.^{6,16,17}

It is the aim of the present work to investigate and to quantify the effect of aleatoric and epistemic uncertainties in reference data on training machine-learned PESs. This is (partially) motivated by earlier findings in which learning on CCSD(T)-F12 data (energies and forces) led to a rapid convergence toward an error floor of several 10⁻⁴ kcal/mol while a lower out-of-sample error was achieved using *ab initio* data of MP2 quality.¹⁸ Inspection of the literature shows that the gradients in MOLPRO at the CCSD(T)-F12 level indeed can be less accurate than machine precision.¹⁹ Additionally, the work explores the effects of convergence criteria required to define in quantum chemical calculations and of using single-reference methods for systems with multi-reference character on the *ab initio* data and subsequent learning. The two molecules considered here are H₂CO and HONO.^{20,21} Both molecules are relevant in atmospheric chemistry and serve as benchmark systems for single- (H₂CO) and multi- (HONO) reference systems from an electronic structure perspective.

The work is organized as follows: first, the methods employed are described. This is followed by results on learning with perturbed energies and with perturbed forces. The role of hyperparameters is briefly considered followed by an exploration of perturbations due to convergence of the electronic structure calculations and multi-reference effects.

2 Methods

This section describes the generation of the datasets and the learning protocols used in the present work. The two molecules considered are H₂CO and HONO. For H₂CO a RKHS representation of reference MP2/aug-cc-pVTZ data is available¹⁸ from which “clean” energies and forces - apart from numerical imprecisions - can be determined. For HONO a recent study²² suggested that training PhysNet on MP2 data - neglecting multi-reference effects in the electronic structure calculations - makes training the NN more cumbersome. Whether or not this observation is related to the neglect of multi-reference effects will be quantitatively assessed in the present work.

2.1 Clean Models and Models with Noise for H₂CO

For H₂CO clean datasets were obtained by evaluating a RKHS representation for 3601 reference geometries.²² Here, clean refers to the notion that apart from numerical imprecisions no further sources of noise arise because for a given geometry the energy is obtained from evaluation of a function based on a matrix-vector multiplication. The kernel coefficients of the RKHS-based^{23,24} PES, available from previous work,¹⁸ were generated by using energies and forces calculated at the MP2/aug-cc-pVTZ level of theory.

To evaluate aleatoric uncertainty arising from effects such as convergence thresholds and/or multi-reference effects in electronic structure calculations, Gaussian-distributed noise with given amplitude was generated and added according to the following procedure. Gaussian random numbers were generated from a distribution with zero mean and three standard deviation (SD = 10⁻⁵, 10⁻⁶ and 10⁻⁷ eV (for energy) and eV/Å (for forces)). For each data point of the clean PES, energy and force perturbations were drawn from the distributions and added to the data point. This leads to six sets of perturbed energies and forces which

are used in addition to the clean dataset to learn representations of the PES using PhysNet.²⁵

2.2 Machine-Learned Potential Energy Surfaces

For all datasets generated and employed in the present work, PhysNet was used to learn a representation of the PES.²⁵ PhysNet is a high-dimensional, message passing NN built to learn molecular properties such as energy and forces from *ab initio* data.²⁵ Starting from the Cartesian coordinates \mathbf{r}_i and nuclear charges z_i of all atoms i of an arbitrary molecular geometry a feature vector is learned to best describe the atoms’ local chemical environment. Atomic energy contributions are then predicted based on the feature vector. The learnable parameters of the NN-based PES are determined by minimizing a suitable loss function

$$\mathcal{L} = w_E |E - E^{\text{ref}}| + \frac{w_F}{3N} \sum_{i=1}^N \sum_{\alpha=1}^3 \left| -\frac{\partial E}{\partial r_{i,\alpha}} - F_{i,\alpha}^{\text{ref}} \right| + \mathcal{L}_{\text{nh}} \quad (1)$$

using AMSGrad.²⁶ Here, E_{ref} and $F_{i,\alpha}^{\text{ref}}$ are the reference energy and the force components for atom i with $(\alpha = x, y, z)$. Parameters w_E and w_F are the weighting parameters (hyperparameters) determining the relative contribution of individual error terms to the loss function and \mathcal{L}_{nh} denotes a “nonhierarchicality penalty” which adds a penalty if the predictions of the individual modules do not decay with increasing depth in the PhysNet architecture.

Six different dataset sizes were considered for training on clean and perturbed energies together with clean and perturbed forces for H₂CO. For training on energies-only the training dataset sizes were $N_{\text{train}} = 500$, to 3000 in steps of 500. For each case the validation dataset size is $\sim 1/8$ of the training dataset size (ranging from $N_{\text{valid}} = 63$ to 375), respectively. The remaining structures from a total dataset size of 3601 constituted the test datasets. Repeat trainings were carried out by maintaining the hyperparameters, training and validation dataset sizes, but varying the initialization.

Learning curves^{27,28} were generated for all clean and perturbed datasets by computing the dataset size dependent root-mean squared errors (RMSEs) for the predicted energy (RMSE(E)) or force (RMSE(F)). In such curves, the lowest and/or the average RMSE of the two training runs for each dataset size are reported. Training of a particular model continued until the performance on the validation set did not improve anymore as judged by the loss, see Eq. 1, or loss on the validation set started to increase again due to overfitting. Typically, the model with the lower RMSE(E) was further analyzed.

2.3 Electronic Structure Calculations

All electronic structure calculations in the present work were carried out using MOLPRO²⁹ or Gaussian09.³⁰ The energies and forces for H₂CO at the 3601 geometries obtained from normal mode sampling³¹ have been determined previously.²² To quantify the uncertainties incurred by converging the Hartree-Fock wavefunction to different thresholds, calculations at the MP2/aug-cc-pVTZ level of theory using the Gaussian09 software package were carried out. The density based convergence limits considered in the SCF were 10^{-8} , 10^{-6} and 10^{-4} . In Gaussian09 the default convergence criterion on the RMS density matrix is 10^{-8} .

For HONO, energies and forces were calculated at the MP2/aug-cc-pVTZ level of theory for 6406 geometries using MOLPRO²⁹ and were previously published.^{22,32} The dataset contains geometries from normal mode sampling at temperatures ranging from $T = 10$ to 2000 K, from NVT simulations run at 1000 K using the semiempirical GFN2-xTB method³³ and geometries along particular normal modes. Electronic structure calculations for HONO at the coupled-cluster level of theory reveal that the molecule possesses multi-reference character for various structures as indicated by analyzing their T_1 characteristic³⁴ determined from CCSD(T) calculations. Additionally, energies for HONO were determined at the

MRCI/aug-cc-pVTZ level following initial complete active space (CAS) calculations with CASSCF(16,12) for a total of 5987 structures. In this case no analytical forces are available (see below).

3 Results

In the following, results for training with clean and perturbed datasets of different sizes are reported. First, the modelled noise is put into perspective by comparing with *ab initio* calculations employing different SCF convergence thresholds. Next, the effect of perturbed energies on the learning is assessed for H₂CO, followed by examining the effect of adding perturbations to the forces. Then, the role of the hyperparameters is considered. Finally, learning in the context of electronic structure calculations is probed by generating datasets from energies based on reference calculations converged to different thresholds in the SCF procedure and by considering multi-reference effects for HONO.

3.1 The Modelled Noise

Quantum chemical calculations at all levels of theory require convergence of certain quantities to within given thresholds. This leads to aleatoric errors that introduce uncertainties in the computed quantities such as energies or forces. For a set of nuclear geometries on which the PES is trained, all reference calculations are ideally guaranteed to have converged to at least within the required convergence threshold. However, for individual geometries there are still differences in the actual value to which convergence has been reached. For example, for H₂CO energies at the MP2/aug-cc-pVTZ level of theory calculated with Gaussian09 the achieved level of convergence ranges from 0.37×10^{-6} to 0.94×10^{-6} for a threshold of 10^{-6} applied to the RMS density matrix.

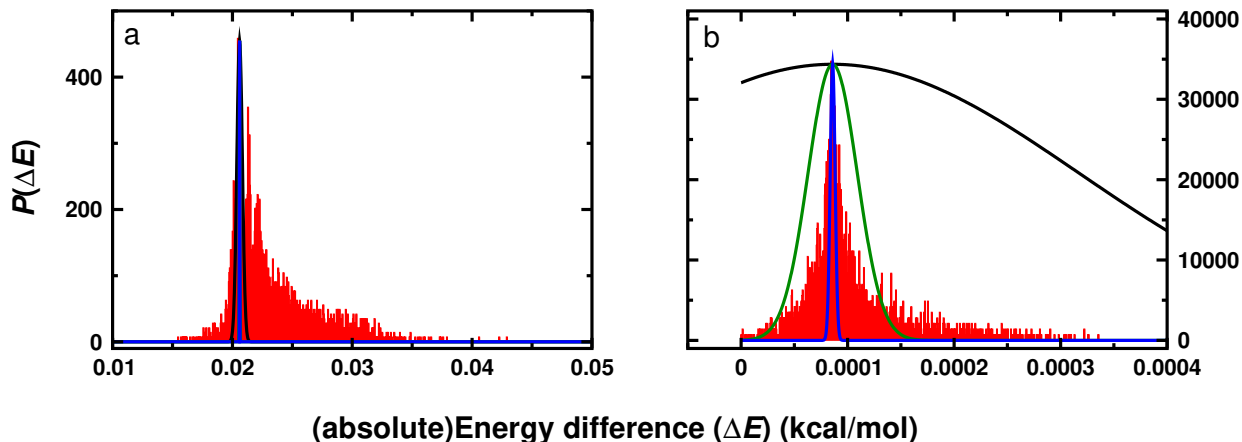


Figure 1: Normalized probability distribution (red histograms) of the absolute energy differences $P(\Delta E)$ between the MP2 energies for H_2CO for 3601 geometries with three (10^{-4} , 10^{-6} and 10^{-8}) different convergence limits in the SCF. The ΔE between energies calculated with SCF convergence limits of 10^{-4} and 10^{-6} is shown in panel a. Panel b shows the result for 10^{-6} and 10^{-8} convergence limits. Both panels also report three Gaussian curves with peak positions fixed at the peak of $P(\Delta E)$ and standard deviations (SDs) of 2.3×10^{-4} (black line), 2.3×10^{-5} (green line) and 2.3×10^{-6} (kcal/mol) (blue line). These SDs correspond to those used to generate random Gaussian noise that was added to the clean $\text{H}_2\text{CO}/\text{RKHS}$ energies and forces.

To put the Gaussian-modelled noise introduced in the methods section and uncertainties in energies arising in quantum chemical calculations into perspective additional *ab initio* calculations for the 3601 geometries of H_2CO used in previous work were carried out.²² All energies were recomputed at the MP2/aug-cc-pVTZ level of theory after converging the SCF wavefunction to within different prescribed convergence criteria. The distribution of energy differences for convergence 10^{-4} and 10^{-6} is reported in Figure 1a and Figure 1b shows the distribution of energy differences with convergence 10^{-6} and 10^{-8} . The distributions are asymmetric with maxima at ~ 0.02 kcal/mol and ~ 0.0001 kcal/mol, respectively.

Superimposed on the distributions in Figures 1a and b are Gaussian distributions centered around the mean with widths 10^{-7} (blue), 10^{-6} (green) and 10^{-5} (black) eV ($\sim 2.3 \times 10^{-6}$ to 2.3×10^{-4} kcal/mol). These correspond to the standard deviations of the generated Gaus-

sian noise. Default convergence criteria used in Gaussian09 are expected to be applicable to typical organic molecules, whereas more lenient convergence criteria of 10^{-4} to 10^{-5} on the density need typically be used for molecules with more challenging electronic structure, such as metal-containing systems.³⁵ For H₂CO using such convergence thresholds lead to a rather wide and asymmetric distribution $P(\Delta E)$ with a long tail towards larger ΔE . It is conceivable that for larger systems, such as [3Fe4S] clusters,³⁵ the distributions $P(\Delta E)$ are at least as broad as the one reported in Figure 1a. For more stringent convergence thresholds (10^{-6} and 10^{-8}) the distribution $P(\Delta E)$ is reported in Figure 1b. This shows that for H₂CO drawing from a Gaussian with SD = 10^{-6} eV is representative, see red histogram and green Gaussian distribution. The more pronounced tail in Figure 1a may imply that using less stringent convergence criteria for the HF-wavefunctions $P(\Delta E)$ is less stochastic whereas for more tightly converged calculations $P(\Delta E)$ is more similar to a Gaussian distribution and the perturbations are more stochastic. It is also noted that with tighter convergence criteria on the density the maximum error shifts to smaller energy differences which is accompanied by narrowing the distribution $P(\Delta E)$. The actual magnitude of the aleatoric uncertainty and the shapes of $P(\Delta E)$ depend on the level of theory used.

It is also found that for higher-energy structures the energy differences from single-point calculations using the two different convergence thresholds increases, see Figures 2a and b. While a general trend suggests that high energy structures tend to exhibit higher uncertainty (ΔE), it is noteworthy that the three structures possessing the highest energies have low ΔE : the three structures with the highest E and ΔE (encircled in Figure 2a) are shown in Figure S1.

The accuracy of PhysNet is estimated to be on the order of $\sim 10^{-3}$ kcal/mol for the present system and data set size. This compares with noise levels of several 0.01 (Figure 2a) and 0.0001 kcal/mol (Figure 2b) from converging the SCF to thresholds between 10^{-4} and 10^{-8} .

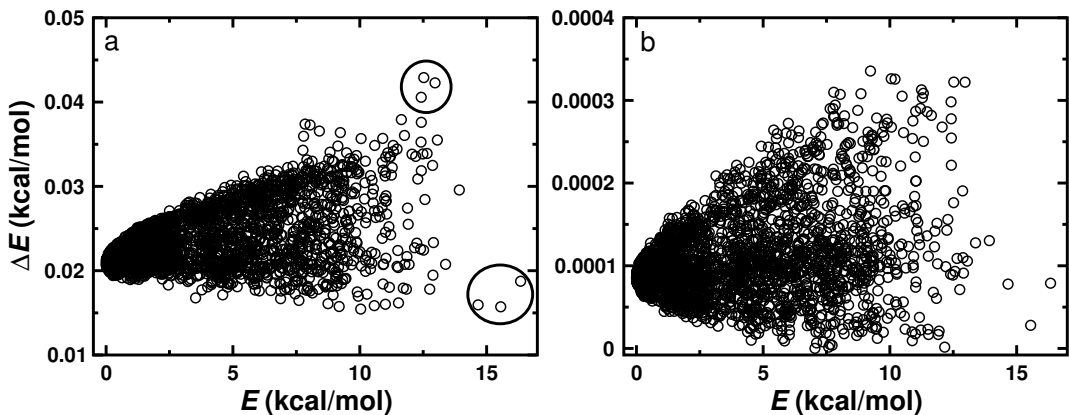


Figure 2: MP2 energy difference ΔE between single point calculations for H_2CO with SCF-convergence 10^{-4} and 10^{-6} (panel a) and SCF-convergence 10^{-6} and 10^{-8} (panel b). The x -axis in both panels are energies from calculations with SCF-convergence 10^{-6} . The black circles mark structures with the highest ΔE and the highest energy and are illustrated in Figure S1.

Hence, while energy fluctuations of 0.01 kcal/mol are somewhat above the accuracy of current ML approaches, achieving a model accuracy on the order of 10^{-4} kcal/mol poses a significant challenge¹⁸ for PESs trained from statistical models.

Similar to the analysis above, threshold-dependent differences can also be obtained for the force components acting on the atoms. The probability distributions of the difference for the x -, y -, and z -components of the forces acting on each of the four atoms for all 3601 geometries of H_2CO with three different convergence limits (10^{-4} , 10^{-6} and 10^{-8}) are shown in Figures 3a and b. As for the energies, these forces were also calculated at the MP2/aug-cc-pVTZ level of theory, using the Gaussian software package.³⁰ Although the peak of the distribution is centered around ~ 0.0 , non-negligible differences are found to either side. Therefore, depending on the convergence criteria used at the SCF step also influences the forces. Furthermore, $\text{SD}=10^{-5}$ eV/Å (2.3×10^{-4} kcal/mol/Å) and $\text{SD}=10^{-6}$ eV/Å (2.3×10^{-5} kcal/mol/Å) used to generate noise on the clean forces fall within the distribution range shown in Figure 3b, but are significantly smaller.

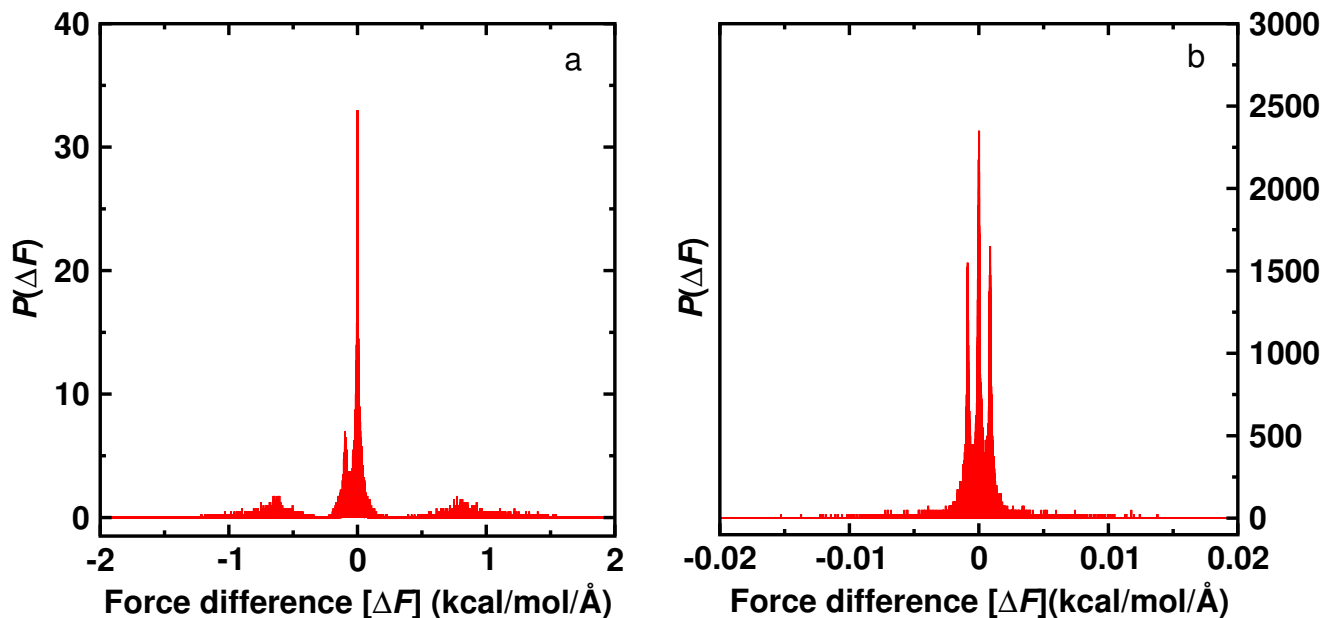


Figure 3: The probability distributions of the differences in force between the MP2 forces, acting on all four atoms, of the H_2CO molecule calculated at 3601 geometries with three (10^{-4} , 10^{-6} and 10^{-8}) different convergence limits in the SCF. The total force differences from calculations with convergence limits 10^{-4} and 10^{-8} are shown in panel a, and panel b reports the results for convergence limits 10^{-6} and 10^{-8} . The probability distributions of (absolute) force differences per atom type (C, O, H) are shown in Figure S2.

3.2 H_2CO : Learning with Perturbed Energies

The learning curves for training PhysNet with “energy-only” for H_2CO are shown in Figure 4. Considering training using only energies (and no forces) is relevant for quantum chemical methods that do not provide analytical gradients, such as multi reference CI methods. Learning curves are reported for the clean dataset and for perturbed energies with amplitudes of 10^{-5} eV (2.3×10^{-4} kcal/mol), 10^{-6} eV (2.3×10^{-5} kcal/mol), and 10^{-7} eV (2.3×10^{-6} kcal/mol). Two independent models were generated for each training dataset size and results are reported for the model with the lower $\text{RMSE}(E)$ (top row) together with the average of the two (bottom row). Figure 4 shows that the learning curves are hardly affected by perturbed energies.

Training based on “energy-only” data without and with perturbation leads to improved

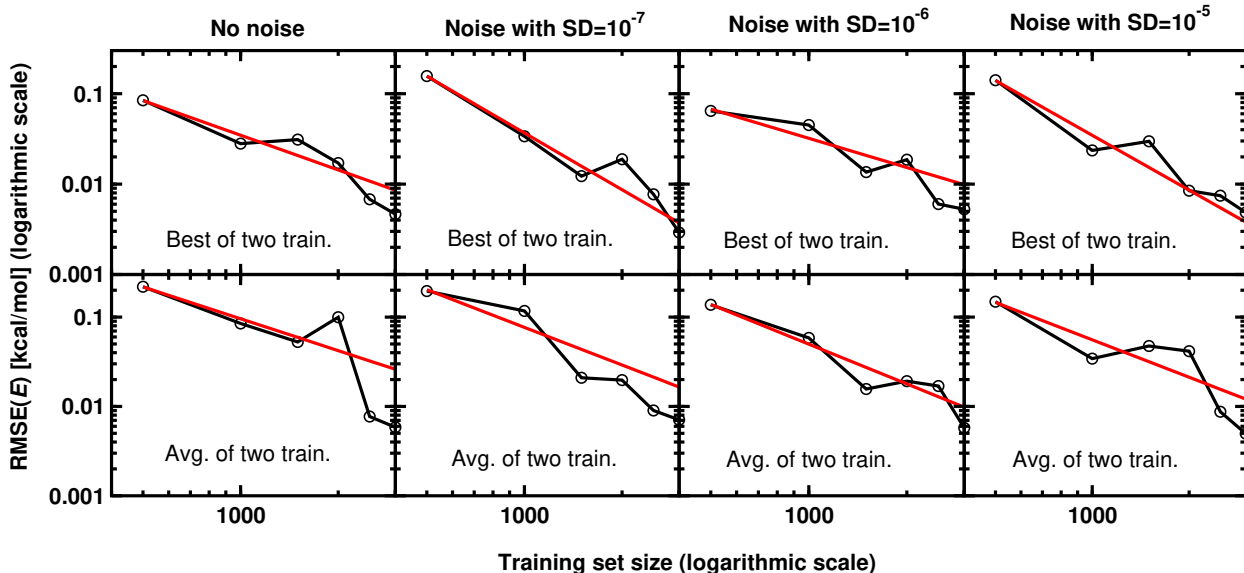


Figure 4: Energy learning curves (log-log plot) on the test data for the PhysNet based models for the H_2CO molecule. The reference energies are the clean RKHS energies and the perturbed RKHS energies with $\text{SD}=10^{-7}$ eV (2.3×10^{-6} kcal/mol), 10^{-6} eV (2.3×10^{-5} kcal/mol) and 10^{-5} eV (2.3×10^{-4} kcal/mol). In each case the models are trained on the same reference data but with dataset sizes of $N_{\text{train}} = 500, 1000, 1500, 2000, 2500$ and 3000 . Top row: performance of the model with the lower $\text{RMSE}(E)$; bottom row: average of the two models.

models with increasing number of training samples and the rate of learning (slope of red lines) is unaffected, in particular for the averaged results. For the clean and perturbed data sets and the different training set sizes $N_{\text{train}} = 500$ and $N_{\text{train}} = 3000$ the [best, worst, average] $\text{RMSE}(E)$ in kcal/mol range from $[0.085; 0.354; 0.219]$ to $[0.005; 0.007; 0.006]$ (clean), $[0.157; 0.234; 0.195]$ to $[0.003; 0.011; 0.007]$ ($\text{SD} = 10^{-7}$ eV), $[0.065; 0.210; 0.138]$ to $[0.005; 0.006; 0.006]$ ($\text{SD} = 10^{-6}$ eV) and $[0.141; 0.157; 0.149]$ to $[0.004; 0.005; 0.005]$ ($\text{SD} = 10^{-5}$ eV). Hence, for small N_{train} addition of noise improves the average $\text{RMSE}(E)$ performance whereas for the largest training data set the performance is virtually indistinguishable. One possible reason is that for the present datasets the training hits the accuracy threshold of the PhysNet architecture/representation which is estimated at $\sim 10^{-3}$ kcal/mol for the present dataset sizes and systems. Therefore, the trained models are insensitive to noise with an amplitude of $< 10^{-4}$ kcal/mol. Note that, on average (i.e. bottom row of Figure 4), the

model with the largest noise performs better than the model without noise. This is likely to be caused by the stochastic nature of NN based approaches and using an ensemble with $N > 2$ or, e.g., using a kernel based method will further clarify the situation.

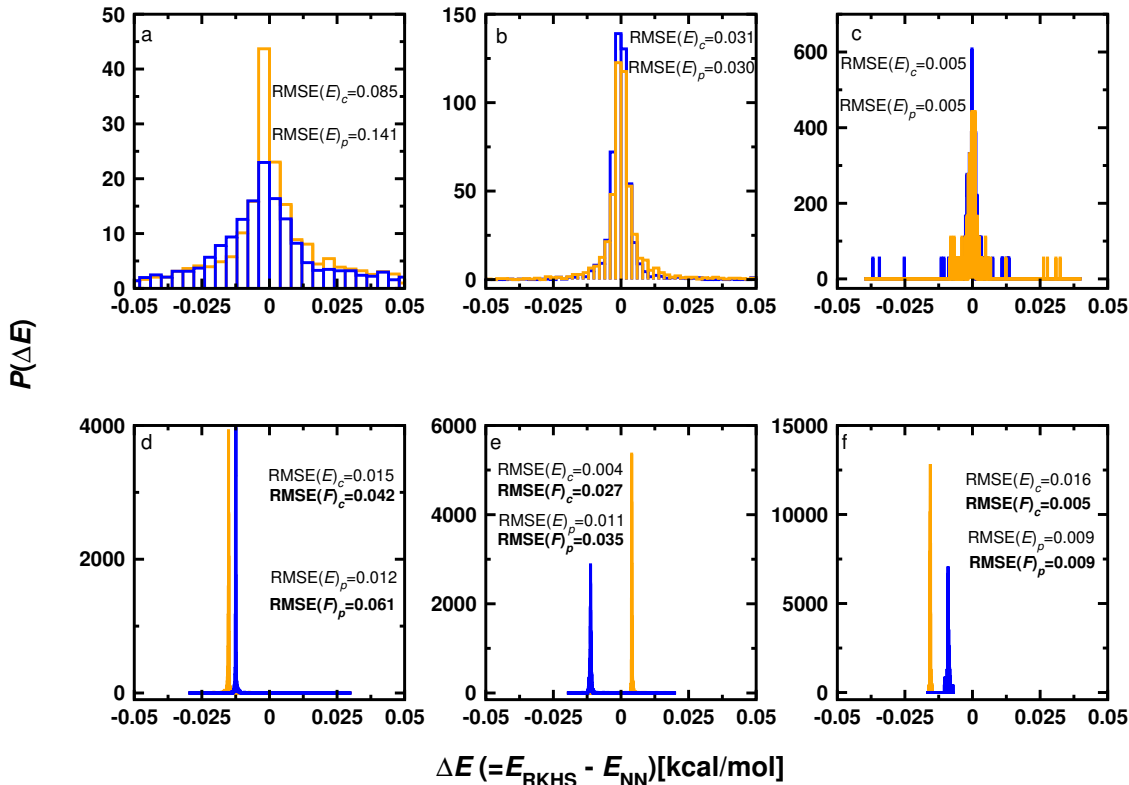


Figure 5: The probability distribution of the energy prediction, $\Delta E = E_{\text{RKHS}} - E_{\text{NN}}$, for $N_{\text{train}} = 500$ (a, d), 1500 (b, e), and 3000 (c, f). Panels a to c: “energy-only” training; perturbed energies contain random Gaussian noise with $\text{SD} = 10^{-5}$ eV (2.3×10^{-4} kcal/mol). Panels d to f: clean energy + force training; perturbed forces contain random Gaussian noise with $\text{SD} = 10^{-5}$ eV/Å (2.3×10^{-4} kcal/mol/Å) and the models are trained with force weighting hyperparameter $w_F \sim 53$ (for trainings with $w_F = 1$ see Figures S4a to c). For each dataset size, the best of the two trainings is shown. $\text{RMSE}(E)_c$ and $\text{RMSE}(E)_p$ represent the root-mean square error in energy for the clean (orange) and noisy (blue) datasets, respectively. $\text{RMSE}(F)_c$ and $\text{RMSE}(F)_p$ are for clean (orange) and noisy (blue) forces. See Figure S3 for $\text{SD} = 10^{-6}$ eV and $\text{SD} = 10^{-6}$ eV/Å on energies and forces, respectively.

It is also of interest to consider energy differences between the predicted E_{NN} and the reference energies E_{RKHS} for the test structures. For learning on “energies-only”, the probability distributions of the energy difference, $\Delta E = E_{\text{RKHS}} - E_{\text{NN}}$, at the test points are shown in

Figures 5a to c for $N_{\text{train}} = 500, 1500$ and 3000 for clean (orange) and perturbed ($\text{SD} = 10^{-5}$ eV (2.3×10^{-4} kcal/mol), blue) data. While this noise level corresponds to an extreme case and is likely not realistic for H_2CO , it is representative for systems with intricate electronic structure. The same assessment was also carried out for a noise level representative of H_2CO ($\text{SD} = 10^{-6}$ eV/ \AA) in Figure S3a to c.

For 500 training samples (Figure 5a), the RMSE between the clean and the perturbed energies for the best models differs by a factor of ~ 2 , i.e. 0.08 and 0.14 kcal/mol. For the worse of the two models the $\text{RMSE}(E)$ is 0.35 and 0.16 kcal/mol for the clean and perturbed data and illustrates the stochastic nature of training NNs. The differences ΔE extend out to 0.5 kcal/mol for training on the perturbed dataset and, using the best models, the probability to find accurate predictions ($\Delta E \sim 0$ kcal/mol) is twice as high for the clean dataset. For a larger training set (1500 samples) the RMSE between reference and PhysNet energies decreases to 0.03 kcal/mol and is the same for clean and perturbed reference data and for the largest training set size considered, the $\text{RMSE}(E)$ is further reduced to 0.005 kcal/mol for training on both clean and noisy data, see Figures 5b and c. The maximum absolute ΔE on the test set encountered for all training datasets using the clean and perturbed data is comparable: 1.6 kcal/mol and 1.4 kcal/mol, respectively.

3.3 H_2CO : Learning with Perturbed Forces

For clean and perturbed forces, PhysNet was trained together with clean energies. Noise was drawn from Gaussian distributions with zero mean and with $\text{SD}=10^{-5}$ eV/ \AA (2.3×10^{-4} kcal/mol/ \AA) to 10^{-7} eV/ \AA (2.3×10^{-6} kcal/mol/ \AA) and the learning curves as log-log plots are shown in Figure 6. As for the energies, the training set size varied between 500 and 3000 in steps of 500 and two independent PhysNet models were trained each. The top panels of Figure 6 report results for the best of the two trained models whereas the bottom row shows

the average of the two independent trainings. The noise levels employed here (2.3×10^{-4} to 2.3×10^{-6} kcal/mol/Å) are at the lower end of what was observed (1 to 0.01 kcal/mol/Å) from quantum chemical calculations using the different convergence criteria, see Figure 3.

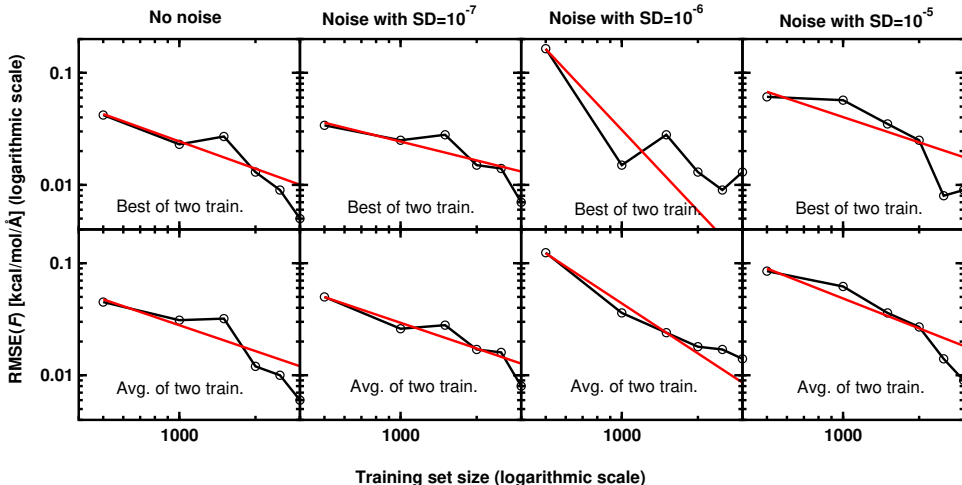


Figure 6: Force learning curves (log-log plot) for PhysNet-based models for H_2CO . The reference forces are the clean RKHS forces (the clean dataset) and the RKHS forces with Gaussian noise of $\text{SD}=10^{-7}$ eV/Å (2.3×10^{-6} kcal/mol/Å), 10^{-6} eV/Å (2.3×10^{-5} kcal/mol/Å) and 10^{-5} eV/Å (2.3×10^{-4} kcal/mol/Å). In each case the models are trained on same reference data but with 500, 1000, 1500, 2000, 2500 and 3000 dataset sizes. Top row: model with lower $\text{RMSE}(E)$; bottom row: average over the two trainings. The energy is the clean RKHS energy and a $w_F \sim 53$ is used (cf., Eq. (1)).

Figure 6 indicates that training models with clean energies and noisy forces can affect the learning curves for the larger noise magnitude ($\text{SD} = 10^{-6}$ eV/Å and 10^{-5} eV/Å). This is unlike for the learning curves using energy-only shown in Figure 4. Therefore, perturbations on the forces may affect the learning of PhysNet more significantly than introducing perturbations on energies.

Training on perturbed forces (with clean energies) yields the probability distributions of the energy difference, $\Delta E = E_{\text{RKHS}} - E_{\text{NN}}$, reported in Figure 5d to f. Here, the spread of $P(\Delta E)$ is invariably smaller than for training on “energy-only” (compare with Figure 5a to c) but the

centroid is shifted slightly away from zero by variable amounts ($[-0.015$ and $-0.012]$, $[0.004$ and $-0.010]$, $[-0.016$ and $0.008]$ kcal/mol). Notably, the energy shift is larger for training on clean data (orange) in two out of three cases, see Figure 5d and f. In this context it is interesting to note that for classification tasks it was found that including measured amounts of noise can improve the generalization capabilities of NN-based models.^{11,12} Possible reasons for the shifts away from $\Delta E = 0$ include i) the energy distributions for training and test set do not center around the same average or ii) training on energies and forces repositions the centroid depending on the weighting w_F in Eq. 1 of the forces, compare Figures 5 and S4.

Concerning point i) it is noted that the average reference energies on the training and test data differ by 0.02, 0.07 and 0.20 kcal/mol for $N_{\text{train}} = 500, 1500$ and 3000. These differences are exactly matched by the trained NNs and compare with differences in the centroids of up to 0.025 kcal/mol in Figure 5d to f. Consequently, differences between average training and test energies seem an unlikely cause. As to point ii) it is found that the centroids for ΔE are at zero for force hyperparameter $w_F = 1$, as will be discussed in more detail below. Hence, the offsets in the energy prediction observed in Figure 5d to f are most likely due to the heavy weight on forces ($w_F \sim 53$) in the training and the fact that reference energies and forces are not fully consistent with one another. Results for training on perturbed data with smaller noise level $\text{SD} = 10^{-6}$ eV/Å (2.3×10^{-5} kcal/mol/Å) are reported in Figure S3.

The $\text{RMSE}(F)$ for training with perturbed forces ($\text{SD} = 10^{-5}$ eV/Å) and clean energies increases with decreasing size of the training data set: $\text{RMSE}(F)_c = 0.005$ and $\text{RMSE}(F)_p = 0.009$ kcal/mol/Å for $N_{\text{train}} = 3000$; 0.027 and 0.035 kcal/mol/Å for $N_{\text{train}} = 1500$; 0.042 and 0.061 kcal/mol/Å for $N_{\text{train}} = 500$, see Figures 5d-f. These compare to $\text{RMSE}(F)_c = 0.007$ and $\text{RMSE}(F)_p = 0.009$ kcal/mol/Å for $N_{\text{train}} = 3000$; 0.037 and 0.037 kcal/mol/Å for $N_{\text{train}} = 1500$; 0.048 and 0.109 kcal/mol/Å for $N_{\text{train}} = 500$ for the inferior models. Thus, training on clean data yields $\text{RMSE}(F)$ which are lower throughout. On the other hand, the

trend is less clear for the energies, for which, e.g., $\text{RMSE}(E)_c = 0.016$ and $\text{RMSE}(E)_p = 0.009$ for a dataset size of 3000. Thus, perturbing the forces of H_2CO with large-amplitude artificial Gaussian noise can impact the learnability and quality of NN-based PESs. This is a particular challenge when NNs are trained from methods without analytical derivatives, such as MRCI+Q. It should also be noted that from a practical perspective clean energies with perturbed forces is a less-likely scenario as perturbed forces are typically expected to originate from perturbations on the energies. On the other hand, forces at the CCSD(T)-F12 level have been found to be less accurate than machine precision³⁶ and lead to “floors” in the learning curve.¹⁸ To more broadly corroborate these findings a larger number of NNs needs to be trained. It will also be of interest to consider alternative methods, e.g. kernel-based methods, which are known to reach lower out of sample errors than PhysNet.¹⁸

3.4 Probing Hyperparameters

The choice of hyperparameters is known to affect training progress and model quality for machine learned models, in particular NNs.^{37,38} This influence is analyzed in the following by considering learning curves (see Figures 7a to d) for the PhysNet-based models resulting from energy+force training for H_2CO using two different values for weighting the force contribution, w_F , in the loss function, see Eq. 1. The energies for training were clean RKHS energies, whereas for the forces clean and Gaussian-perturbed forces (largest amplitude $\text{SD} = 10^{-5} \text{ eV}/\text{\AA} = 2.3 \times 10^{-4} \text{ kcal/mol}/\text{\AA}$) were used. The two force weighting hyperparameters were $w_F \sim 53$ and $w_F = 1$. Figures 7a and b show that for a large value of the hyperparameter $w_F \sim 53$ the error in the energy prediction does not decrease linearly with increasing dataset size for both, clean and perturbed forces. This changes if the value of the hyperparameter is decreased to $w_F = 1$, see Figures 7c and d: without noise the learning curve drops monotonically for almost all training data set sizes (panel c) whereas with noise present first a plateau is found after which a largely monotonous decrease follows (panel d).

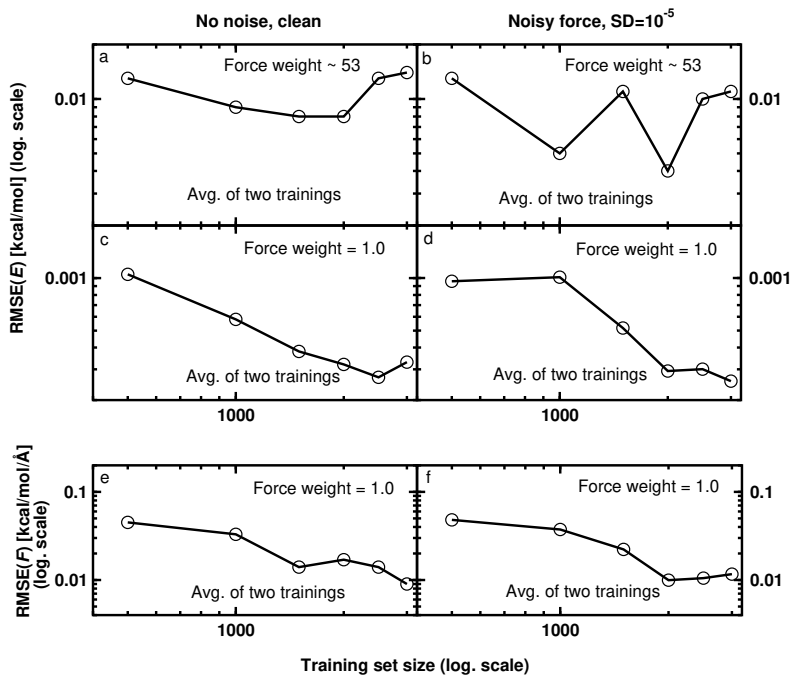


Figure 7: Panels a-d: The energy learning curves for the PhysNet based models for the H_2CO molecule as log-log plot. The reference energies are the clean RKHS energies whereas the reference forces are the clean RKHS forces and the forces with Gaussian noise with $\text{SD}=10^{-5}$ eV/Å (2.3×10^{-4} kcal/mol/Å). The used value of the weighting parameter of force in the loss function (cf., Eq. (17) of Ref. 25) during training are $w_F \sim 53$ (cf., panels a and b) and $w_F = 1$ (cf., panels c and d). Panels e and f: Force learning curves as shown in Figure 6 but only for the clean RKHS forces and forces with Gaussian noise with $\text{SD}=10^{-5}$ eV/Å (2.3×10^{-4} kcal/mol/Å). The used value of the weighting parameter in the loss function during training is $w_F = 1$. The results presented in panels a-f are averaged over two independent trainings.

Corresponding force learning curves with a value of $w_F = 1$ for the hyperparameter are shown in Figures 7e and f. As judged from the $\text{RMSE}(F)$ no effect from introducing noise on the forces is visible and the performance of the two models is almost identical. A comparison of these results with the curves in the bottom row of Figure 6 reveals that the effect of the hyperparameter value on learning the forces is not as severe as it is for the energies. Furthermore, the probability distributions $P(\Delta E)$ for the prediction error using $w_F = 1$ do not exhibit appreciable shifts away from $\Delta E = 0$, see Figure S4, which differs from the findings for trainings with $w_F \sim 53$ as in Figure 5. Hence, heavier weighting of force components in

the present case leads to small but noticeable displacements of the average predicted energies. It is noteworthy to mention that the H_2CO vibrational frequencies calculated from the trained models with $w_F = 1$ and $w_F \sim 53$ only differ by a maximum of 0.2 cm^{-1} , i.e. the quality of the trained models only insignificantly depends on the choice of hyperparameter.

3.5 Perturbations from Multi-Reference Effects

Electronic structure calculation require certain input from the user that influence the resulting uncertainties in the computed quantities, such as energies or forces. This includes, e.g., aleatoric uncertainties introduced by convergence criteria on the SCF density and epistemic errors due to smaller or larger basis sets used in the calculations. Furthermore, perturbations can also originate from multi-reference effects. Recently, a detailed investigation of isomerization and decomposition processes of HONO and HNO_2 has been carried out.³⁹ State-of-the-art electronic structure theory was used to compute the HNO_2 PES at the CASPT2 and/or MRCI+Q levels for the dissociation pathways leading to $\text{H}+\text{NO}_2$ and $\text{OH}+\text{NO}$. It was specifically noted that single determinant methods are not reliable due to the presence of low-lying excited states. Therefore, HONO was considered a suitable small molecule to assess the influence of perturbations arising from multi-reference effects in the input data for training PhysNet.

In the following, the T_1 diagnostic was used to quantify the amount of nondynamic electron correlation and whether or not employing a single-reference treatment is appropriate.³⁴ Typically, a value of $T_1 > 0.02$ is taken as an indication that a multi-reference approach should be employed for a particular geometry.³⁴ Alternatively, the D_1 diagnostic could also be used which was, however, not done in the present work.⁴⁰ In addition to the electronic structure calculations of HONO at the MP2/aug-cc-pVTZ level (see Methods), CCSD(T)/aug-cc-pVTZ calculations were carried out to obtain the T_1 amplitudes. The distribution of T_1

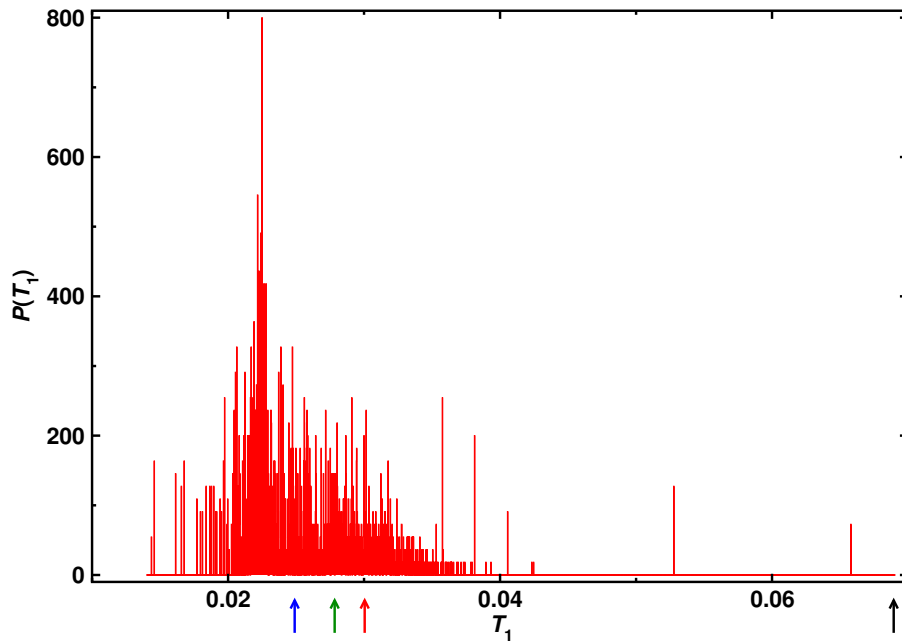


Figure 8: The probability distribution of T_1 values of HONO from CCSD(T)/aug-cc-pVTZ calculations for 3375 geometries. The maximum value of T_1 found in the considered 3375, 2875, 2375 and 1875 structures are ~ 0.070 , ~ 0.030 , ~ 0.028 , ~ 0.025 , respectively. These are indicated here by black, red, green and blue arrows. The broad distribution is akin to an aleatoric uncertainty.

values (for 3375 HONO structures) reported in Figure 8 demonstrates that a multi-reference treatment is required for 3235 ($\sim 96\%$) of these geometries if the criterion $T_1 > 0.02$ is used.

In the following it is of interest to determine whether training PhysNet on subsets of the entire MP2 data set of energies a) displays differences in the learning curves depending on how many energies with multi-reference character (as per the T_1 amplitude) are retained and b) how the model performance is influenced. To this end, the training set for HONO was restricted to structures with progressively lower T_1 amplitudes. This resulted in datasets with 2875 ($T_1 \leq 0.03$), 2375 ($T_1 \leq 0.028$), and 1875 ($T_1 \leq 0.025$) structures. The parts of the distribution $P(T_1)$ that were retained for training are to the left of the colored arrows in Figure 8.

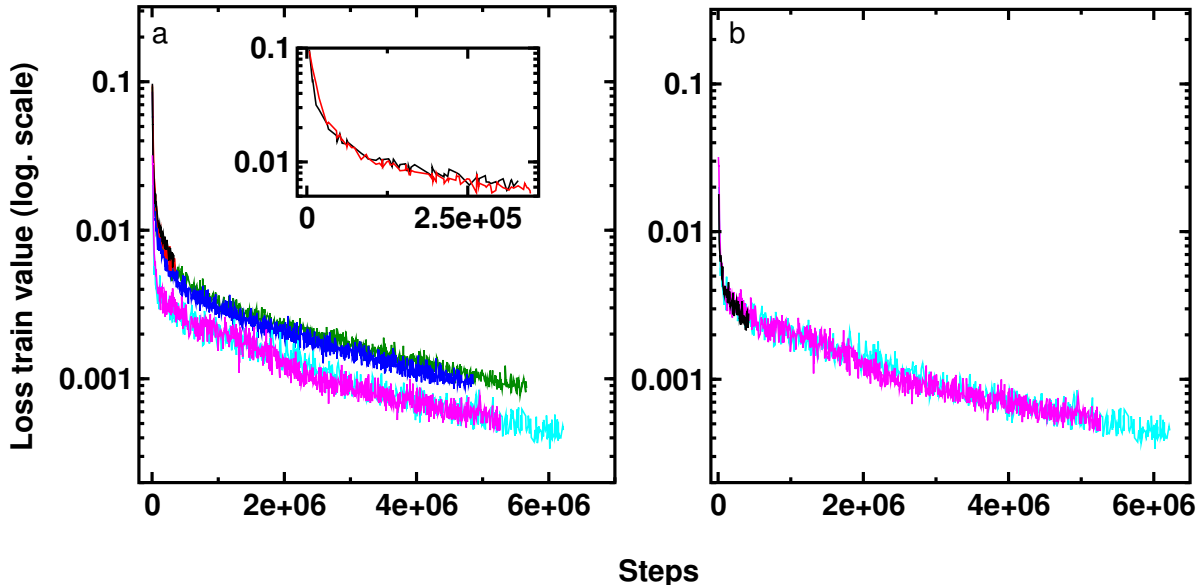


Figure 9: The values of the loss function (training on energy-only) for HONO (panel a and inset) and H₂CO (panels a and b) using different MP2 training dataset sizes up to the point at which overfitting starts. Panel a: The loss function value for HONO from training datasets with 3000 (black, all), 2500 (red, $T_1 \leq 0.030$), 2066 (green, $T_1 \leq 0.028$) and 1631 (blue, $T_1 \leq 0.025$) structures. Panel b: The loss function value for H₂CO with 3000 (cyan), 1500 (magenta) and 500 (black) training dataset sizes. In panel a, results for training with 3000 (cyan) and 1500 (magenta) reference structures for H₂CO are also shown for comparison. The inset in panel a is a close-up for HONO for 3000 and 2500 training set sizes.

Training for each of these datasets was carried out using 87 % training structures and 13 % for validation, and the training loss is shown up to the point for which convergence is reached, *i.e.* the validation loss does not decrease further or even increases again due to overfitting. The value of the loss function for HONO (calculated on the training data) is reported in Figure 9a. If structures with $T_1 \leq 0.03$ (red trace) are retained, the loss is similar to the one for using the entire dataset (black trace) without restriction on structures with particular T_1 amplitude, see also inset in Figure 9a. The value of the loss function reaches ~ 0.006 for these two training dataset sizes after $\sim 3 \times 10^5$ steps. However, for progressively tighter criteria on structures with lower T_1 amplitudes (green and blue traces), training continues for at least one order of magnitude more steps ($\sim 5 \times 10^6$) and reaches lower values for the loss function by about a factor of 5.

Similarly, training on MP2 energies for H₂CO using 500, 1500, and 3000 training structures were carried out and the value of the loss function is reported in Figure 9b (black, magenta, cyan). Here it is found that with the smallest training set the loss function improves for about one order of magnitude fewer steps compared with the two larger training set sizes. This differs for HONO in that the largest training set size was found to stop learning first. For direct comparison with HONO, the magenta and cyan traces (H₂CO for 1500 and 3000 training data from panel b) are also reported in Figure 9a. This demonstrates that by eliminating structures with high T_1 from the HONO data set but retaining a sufficiently large training data set size (≥ 1500 structures) the loss function decays in a comparable fashion as for the H₂CO MP2 energies which do not contain potential noise from multi-reference calculations. Hence, the presence of energies for structures with multi-reference character, but treated with a single-reference method, compromises the learning capabilities of a model such as PhysNet. Overall, however, the rate at which the loss function decays and the best achievable model are inferior to training on a dataset of clean, single-reference energies such as for H₂CO. One possibility is that - as is the case for HONO - the mixture of energies that are or are not affected by multi-reference effects, as measured by the T_1 amplitude, leads to difficulties in the learning, which is considered next.

For this it was assessed whether the total energy of a particular structure, the prediction error, and T_1 are correlated. Again, the MP2 data sets for HONO with progressively lower T_1 amplitudes was considered. Figure 10a reports the results from training PhysNet using all MP2 reference data, i.e. without restriction on T_1 values. Qualitatively it is found that large values of T_1 are associated with high energy structures. The converse is not necessarily true: there are also high-energy structures that do exhibit only moderately large T_1 amplitudes. Large positive (red density) and negative (blue density) prediction errors arise and are typically associated with high-energy structures and/or large values of T_1 . These

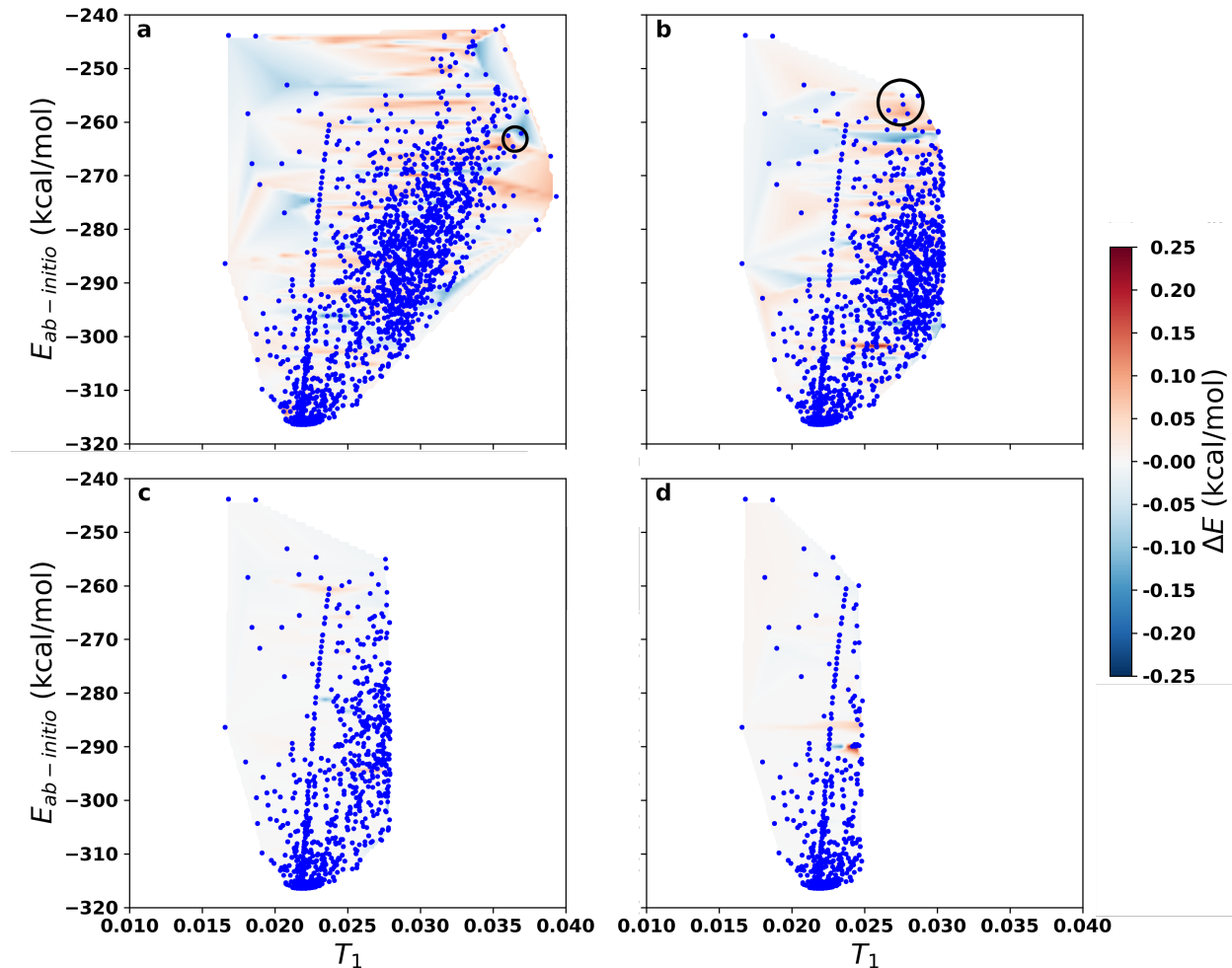


Figure 10: Heatmap for the error distribution $\Delta E = E_{\text{ref}} - E_{\text{NN}}$ for HONO trained on MP2 energies depending on the T_1 amplitude (from CCSD(T)/aug-cc-pVTZ calculations) and the total energy of a structure $E_{\text{ab-initio}}$. Panel a: without restriction on the T_1 amplitude; panel b: $T_1 \leq 0.030$; panel c: $T_1 \leq 0.028$; panel d: $T_1 \leq 0.025$. Dark red and blue regions only occur if structures with $T_1 \geq 0.028$ are retained in the training. Structures for the encircled data points in panels a and b are reported in Figure S6. For the probability distributions $p(\Delta E)$, see Figure S5. Note that single outliers with larger $|\Delta E|$ are excluded for clarity.

prediction errors are skewed towards $\Delta E > 0$ (red), see also inset in Figure S5. Restricting the training set to structures with $T_1 \leq 0.030$ leads to the performance reported in Figure 10b. Large positive (dark red) and negative (dark blue) errors for the energy still occur. For the training in Figure 10c only structures with $T_1 \leq 0.028$ were retained which considerably reduces large positive prediction errors and no large negative errors are found anymore. The correlation between the magnitude of T_1 and the magnitude of the prediction error is further corroborated by training on structures with yet smaller $T_1 \leq 0.025$, see Figure 10d. Consequently, the widths for the prediction errors decrease considerably, see Figure S5. In summary, this analysis points to a direct relationship between the magnitude of T_1 and the prediction errors from models trained on corresponding subsets.

Structures with particularly high T_1 and large prediction errors are encircled in Figures 10a and b and the corresponding geometries are reported in Figures S6 and S7. It is found that in all cases the geometries are perturbed away from the HONO equilibrium geometry in a pronounced fashion. For example, the structure with 116.4° dihedral angle (see Figure S6a) has a noticeably longer $R_{\text{O}_\text{B}\text{H}}$ bond length and widely open $\theta_{\text{O}_\text{A}\text{N}\text{O}_\text{B}}$; the structure with -72.7° dihedral angle (see Figure S6b) has longer bond lengths for all three bonds, whereas the structure with 58.2° dihedral angle has a narrow $\theta_{\text{O}_\text{A}\text{N}\text{O}_\text{B}}$ angle.

Finally, it is also of interest to compare the final model performance on the training and test sets for reference MP2 and MRCI+Q calculations, see Table 1, which addresses epistemic errors. Here, it was found that the $\text{RMSE}(E)$ on the training set increased by about an order of magnitude in going from MP2 to MRCI+Q reference data, largely irrespective of the size of the training set N_{train} . This does not translate directly to model performance on the test data. In this case the trained models differ rather by a factor of 2 to 3 for MP2 vs. MRCI+Q reference data. Nevertheless, training on the MRCI+Q reference calculations yields models with higher representation errors in comparison to those trained on MP2 data.

Conversely, training a single-reference problem such as H₂CO on MP2 reference data leads to models that are more accurate by an order of magnitude compared with a multi-reference system (HONO) using the same single-reference method (MP2). Besides effects from single-/multi-reference H₂CO is a molecule with higher symmetry and the energy range of the employed dataset is smaller by a factor of ~ 5 (energy range of ~ 15 kcal/mol for H₂CO vs. 80 kcal/mol for HONO), which presumably make the learning process easier for H₂CO.

Table 1: Summary of the "energy-only" trainings for H₂CO (MP2) and HONO (*MP2, **MRCI+Q) along with the root-mean squared errors for the energy (rounded to six decimal place) on the training (RMSE(E)_{train}) and test (RMSE(E)_{test}) data given in kcal/mol. *Average of five independent trainings with different seeds.**

Compound	N_{tot}	N_{train}	N_{valid}	N_{test}	RMSE(E) _{train}	RMSE(E) _{test}
H ₂ CO	3601	3000	375	226	0.002858	0.005601
H ₂ CO	3601	1500	188	1913	0.003789	0.019181
HONO* (full)	6406	3000	375	3031	0.051401	0.164302
HONO* ($T_1 \leq 0.030$)	2875	2300	288	287	0.025900***	0.233161***
HONO* ($T_1 \leq 0.030$)	2875	2500	375	0	0.057809	n.a.
HONO* ($T_1 \leq 0.028$)	2375	1900	238	237	0.020399***	0.291417***
HONO* ($T_1 \leq 0.028$)	2375	2066	309	0	0.006552	n.a.
HONO* ($T_1 \leq 0.025$)	1875	1500	188	187	0.016898***	0.290245***
HONO* ($T_1 \leq 0.025$)	1875	1631	244	0	0.005003	n.a.
HONO**	3150	2520	315	315	0.155482***	0.434823***
HONO**	3150	2205	276	669	0.131824	0.358221
HONO**	3150	1890	236	1024	0.132721	0.579272
HONO**	3150	1575	197	1378	0.165319	0.716033

4 Conclusions

In this contribution the effect of perturbations in the reference data obtained from quantum chemistry calculations used for training ML-based potential energy surfaces is quantified. The work explores the effects of a) convergence criteria in quantum chemical calculations and b) using single-reference methods for systems with multi-reference character on the *ab*

initio data and subsequent learning. H₂CO is a small, symmetric and closed-shell molecule for which high-quality reference calculations for structures around the minimum geometry are standard. Changing the convergence limits of the SCF calculations to those typical of larger and electronically more demanding systems, such as metal-complexes, may affect the trainability of PhysNet if perturbations are present in the forces. Nevertheless, for perturbed forces the effects on the trained NNs found in the present work were still comparatively small although the magnitude of the perturbations used on the clean data was rather small compared with what is found from quantum chemical calculations employing difference convergence thresholds in the SCF calculations. It is possible that with alternative ML strategies, such as the kernel-based Faber/Christensen/Huang/von Lilienfeld (FCHL) approach,^{41,42} lower representation errors can be reached and the noise floor is detected earlier and even "energy-only" learning is sensitive to perturbations in the data.

For HONO, which requires a multi-reference treatment, a clear correlation between the accuracy of the final model and the T_1 amplitude - which is a measure of nondynamic correlation - was found, see Figure 10. Furthermore, the quality of the models as judged from the RMSE(E) on the training and test data set, clearly differs between H₂CO and HONO at the MP2 levels of theory. These effects are even more pronounced when comparing model performance for HONO on MP2 and MRCI+Q reference data, see Table 1.

Within a broader scope, multi-reference CI and second order perturbation theory (CASPT2) calculations require the definition of an "active space" of molecular orbitals that are treated within the multi-reference calculation. Usually, the orbitals that constitute the active space are not uniquely defined. For example, which orbitals to retain in the active space and whether or not to introduce new orbitals may well change for an ensemble of molecular structures. Hence, it is expected that working with one definition of the CAS for reactions - an ensemble of structures including reactant, product, and transition state(s) - a union of

orbitals specific for each structure should be employed for a balanced treatment. This necessarily increases the CAS and renders routine calculations for larger molecules impractical. Furthermore, the simulation of excited states for one of these structures would require yet another set of orbitals for the active space. This freedom in choosing suitable orbitals for an ensemble of structures introduces epistemic uncertainty into such calculations whereas the fact that for a given set of orbitals the weight of each Slater-determinant changes leads to aleatoric uncertainty.

It is of interest to note that far away from the minimum energy structure and for electronically more demanding systems, e.g. those containing metal centers or halogens, multi-reference effects are rather the norm than the exception.⁴³ Therefore, training machine learning models - in particular neural networks as was done in the present work - requires circumspection in assessing the role of noise, both aleatoric and epistemic, when assessing model performance. Finally, it is important to mention that further work is required for a broader and more comprehensive understanding and characterization of what role noise/errors in the input data plays for the performance of NN-based PESs.

Acknowledgment

Support by the Swiss National Science Foundation through grants 200021_117810, 200021_215088, the NCCR MUST (to MM), and the University of Basel is acknowledged. This work was also supported by the United State Department of the Air Force, which is gratefully acknowledged (to MM). This project has received funding from European Union's Horizon 2020 under MCSA Grant No 801459, FP-RESOMUS. Valuable correspondence on complete active spaces with Prof. R. Lindh is acknowledged.

Data Availability Statement

The clean and perturbed RKHS energies and all reference data employed in the present study are available at <https://github.com/MMunibas/noise>.

References

- (1) Unke, O. T.; Chmiela, S.; Sauceda, H. E.; Gastegger, M.; Poltavsky, I.; Schütt, K. T.; Tkatchenko, A.; Müller, K.-R. Machine learning force fields. *Chem. Rev.* **2021**, *121*, 10142–10186.
- (2) Manzhos, S.; Carrington Jr, T. Neural network potential energy surfaces for small molecules and reactions. *Chem. Rev.* **2021**, *121*, 10187–10217.
- (3) Meuwly, M. Machine Learning for Chemical Reactions. *Chem. Rev.* **2021**, *121*, 10218–10239.
- (4) Vapnik, V. N. *Statistical Learning Theory*; Wiley-Interscience, 1998.
- (5) Koner, D.; Bemish, R. J.; Meuwly, M. The $C(^3P) + NO(X^2\Pi) \rightarrow O(^3P) + CN(X^2\Sigma^+)$, $N(^2D)/N(^4S) + CO(X^1\Sigma^+)$ reaction: Rates, branching ratios, and final states from 15 K to 20 000 K. *J. Chem. Phys.* **2018**, *149*, 094305.
- (6) Veliz, J. C. S. V.; Koner, D.; Schwilk, M.; Bemish, R. J.; Meuwly, M. The $C(^3P) + O_2(^3\Sigma_g^-) \rightarrow CO_2 \leftrightarrow CO(^1\Sigma^+) + O(^1D)/O(^3P)$ reaction: thermal and vibrational relaxation rates from 15 K to 20000 K. *Phys. Chem. Chem. Phys.* **2021**, *23*, 11251–11263.
- (7) Käser, S.; Unke, O. T.; Meuwly, M. Reactive dynamics and spectroscopy of hydrogen transfer from neural network-based reactive potential energy surfaces. *New J. Phys.* **2020**, *22*, 055002.

- (8) Qu, C.; Conte, R.; Houston, P. L.; Bowman, J. M. Full-dimensional potential energy surface for acetylacetone and tunneling splittings. *Phys. Chem. Chem. Phys.* **2021**, *23*, 7758–7767.
- (9) Van Gorp, J.; Schoukens, J.; Pintelon, R. Learning neural networks with noisy inputs using the errors-in-variables approach. *IEEE Transactions on Neural Networks* **2000**, *11*, 402–414.
- (10) Goldberger, J.; Ben-Reuven, E. Training deep neural-networks using a noise adaptation layer. International conference on learning representations. 2016.
- (11) Gardner, E.; Wallace, D.; Stroud, N. Training with noise and the storage of correlated patterns in a neural network model. *Journal of Physics A: Mathematical and General* **1989**, *22*, 2019.
- (12) Benedetti, M.; Ventura, E. Training neural networks with structured noise improves classification and generalization. *arXiv preprint arXiv:2302.13417* **2023**,
- (13) Valdenegro-Toro, M.; Mori, D. S. A deeper look into aleatoric and epistemic uncertainty disentanglement. In 2022 IEEE. CVF Conference on Computer Vision and Pattern Recognition Workshops (CVPRW). 2022; pp 1508–1516.
- (14) Saunders, V.; Hillier, I. A “Level-Shifting” method for converging closed shell Hartree–Fock wave functions. *Int. J. Quant. Chem.* **1973**, *7*, 699–705.
- (15) Koner, D.; Veliz, J. C. S. V.; van der Avoird, A.; Meuwly, M. Near dissociation states for $\text{H}_2^+ - \text{He}$ on MRCI and FCI potential energy surfaces. *Phys. Chem. Chem. Phys.* **2019**, *21*, 24976–24983.
- (16) San Vicente Veliz, J. C.; Koner, D.; Schwilk, M.; Bemish, R. J.; Meuwly, M. The $\text{N}(^4S) + \text{O}_2(X^3\Sigma_g^-) \leftrightarrow \text{O}(^3P) + \text{NO}(X^2\Pi)$ Reaction: Thermal and Vibrational Relaxation Rates for the $^2A'$, $^4A'$ and $^2A''$ States. *Phys. Chem. Chem. Phys.* **2020**, *22*, 3927–3939.

- (17) Koner, D.; Veliz, J. C. S. V.; Bemish, R. J.; Meuwly, M. Accurate Reproducing Kernel-Based Potential Energy Surfaces for the Triplet Ground States of N₂O and Dynamics for the N+NO \leftrightarrow O+N₂ Reaction. *Phys. Chem. Chem. Phys.* **2020**, *22*, 18488–18498.
- (18) Käser, S.; Koner, D.; Christensen, A. S.; von Lilienfeld, O. A.; Meuwly, M. Machine learning models of vibrating H₂CO: Comparing reproducing kernels, FCHL, and PhysNet. *J. Phys. Chem. A* **2020**, *124*, 8853–8865.
- (19) Györfy, W.; Werner, H.-J. Analytical energy gradients for explicitly correlated wave functions. II. Explicitly correlated coupled cluster singles and doubles with perturbative triples corrections: CCSD (T)-F12. *J. Chem. Phys.* **2018**, *148*, 114104.
- (20) Kasting, J. F. Earth’s early atmosphere. *Science* **1993**, *259*, 920–926.
- (21) Finlayson-Pitts, B. J.; Pitts Jr, J. N. Atmospheric chemistry. Fundamentals and experimental techniques. **1986**,
- (22) Käser, S.; Boittier, E. D.; Upadhyay, M.; Meuwly, M. Transfer Learning to CCSD(T): Accurate Anharmonic Frequencies from Machine Learning Models. *J. Chem. Theor. Comp.* **2021**, *17*, 3687–3699.
- (23) Ho, T.-S.; Rabitz, H. A General Method for Constructing Multidimensional Molecular Potential Energy Surfaces from Ab Initio Calculations. *J. Chem. Phys.* **1996**, *104*, 2584–2597.
- (24) Unke, O. T.; Meuwly, M. Toolkit for the Construction of Reproducing Kernel-Based Representations of Data: Application to Multidimensional Potential Energy Surfaces. *J. Chem. Inf. Model.* **2017**, *57*, 1923–1931.
- (25) Unke, O. T.; Meuwly, M. PhysNet: A Neural Network for Predicting Energies, Forces, Dipole Moments, and Partial Charges. *J. Chem. Theor. Comp.* **2019**, *15*, 3678–3693.

- (26) Reddi, S.; Kale, S.; Kumar, S. On the convergence of ADAM and beyond. International conference on learning representations. 2018.
- (27) Cortes, C.; Jackel, L. D.; Solla, S.; Vapnik, V.; Denker, J. Learning curves: Asymptotic values and rate of convergence. *Adv. Neur. Inf. Proc. Sys.* **1993**, *6*.
- (28) Müller, K.-R.; Finke, M.; Murata, N.; Schulten, K.; Amari, S.-i. A numerical study on learning curves in stochastic multilayer feedforward networks. *Neur. Comput.* **1996**, *8*, 1085–1106.
- (29) Werner, H.-J.; Knowles, P. J.; Knizia, G.; Manby, F. R.; Schütz, M. *Wiley Interdiscip. Rev.: Comput. Mol. Sci.* **2012**, *2*, 242–253.
- (30) Frisch, M. J.; Trucks, G. W.; Schlegel, H. B.; Scuseria, G. E.; Robb, M. A.; Cheeseman, J. R.; Scalmani, G.; Barone, V.; Mennucci, B.; Petersson, G. A. et al. Gaussian 09 Revision D.01. Gaussian Inc. Wallingford CT 2009.
- (31) Smith, J. S.; Isayev, O.; Roitberg, A. E. ANI-1, A data set of 20 million calculated off-equilibrium conformations for organic molecules. *Sci. data* **2017**, *4*, 1–8.
- (32) Käser, S.; Boittier, E.; Upadhyay, M.; Meuwly, M. VibML. 2021; <https://doi.org/10.5281/zenodo.4585449>.
- (33) Bannwarth, C.; Ehlert, S.; Grimme, S. GFN2-xTB—An accurate and broadly parametrized self-consistent tight-binding quantum chemical method with multipole electrostatics and density-dependent dispersion contributions. *J. Chem. Theor. Comp.* **2019**, *15*, 1652–1671.
- (34) Lee, T. J.; Taylor, P. R. A diagnostic for determining the quality of single-reference electron correlation methods. *Int. J. Quantum Chem.* **1989**, *36*, 199–207.

- (35) Meuwly, M.; Karplus, M. Theoretical investigations on *Azotobacter vinelandii* ferredoxin I: effects of electron transfer on protein dynamics. *Biophys. J.* **2004**, *86*, 1987–2007.
- (36) Győrffy, W.; Werner, H.-J. Analytical energy gradients for explicitly correlated wave functions. II. Explicitly correlated coupled cluster singles and doubles with perturbative triples corrections: CCSD (T)-F12. *J. Chem. Phys.* **2018**, *148*.
- (37) Liao, L.; Li, H.; Shang, W.; Ma, L. An empirical study of the impact of hyperparameter tuning and model optimization on the performance properties of deep neural networks. *ACM Trans. Softw. Eng. Methodol.* **2022**, *31*, 1–40.
- (38) Yuan, Y.; Wang, W.; Pang, W. A systematic comparison study on hyperparameter optimisation of graph neural networks for molecular property prediction. Proceedings of the Genetic and Evolutionary Computation Conference. 2021; pp 386–394.
- (39) Chen, X.; Fuller, M. E.; Goldsmith, C. F. Decomposition kinetics for HONO and HNO₂. *React. Chem. Eng.* **2019**, *4*, 323–333.
- (40) Janssen, C. L.; Nielsen, I. M. New diagnostics for coupled-cluster and Møller–Plesset perturbation theory. *Chem. Phys. Lett.* **1998**, *290*, 423–430.
- (41) Faber, F. A.; Christensen, A. S.; Huang, B.; Von Lilienfeld, O. A. Alchemical and structural distribution based representation for universal quantum machine learning. *J. Chem. Phys.* **2018**, *148*.
- (42) Christensen, A. S.; Bratholm, L. A.; Faber, F. A.; Anatole von Lilienfeld, O. FCHL revisited: Faster and more accurate quantum machine learning. *J. Chem. Phys.* **2020**, *152*.
- (43) Wang, J.; Manivasagam, S.; Wilson, A. K. Multireference character for 4d transition metal-containing molecules. *J. Chem. Theor. Comp.* **2015**, *11*, 5865–5872.

Supporting Information: On the Effect of Aleatoric and Epistemic Errors on the Learnability and Quality of NN-based Potential Energy Surfaces

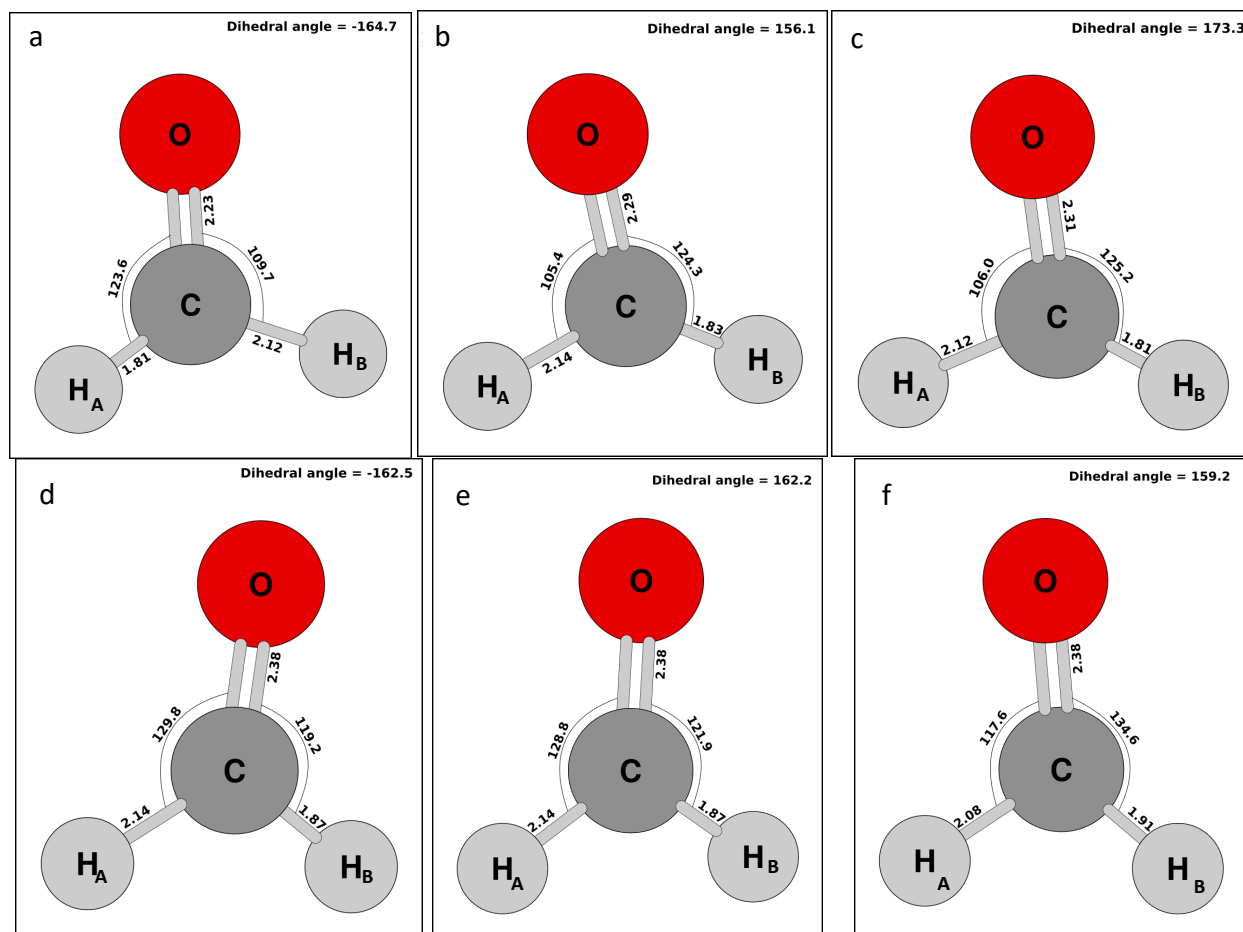


Figure S1: Structures for H_2CO corresponding to data points encircled in Figure 2a. Panels a to c: Structures for data points with $E > 14$ kcal/mol. Panels d to f: structures with $\Delta E > 0.04$ kcal/mol. The distances and angles are in a_0 and degree units, respectively. The equilibrium (MP2/aug-cc-pvtz) structure of H_2CO is planar (dihedral of 180°) with $R_{\text{CO}} = 2.29 a_0$, $R_{\text{CH}} = 2.08 a_0$, $\theta_{\text{OCH}} = 121.7^\circ$. Thus all these six structures are distorted from the equilibrium geometry. Apart from the dihedral angle, the distortion for the structures in panels a to c primarily occurs due to shortening of one of the CH bonds and narrowing of one of the θ_{OCH} angles. On the other hand, distortion for the bottom row (d-f) structures primarily takes place because of shortening of one of the CH bonds and opening up of one of the θ_{OCH} angles.

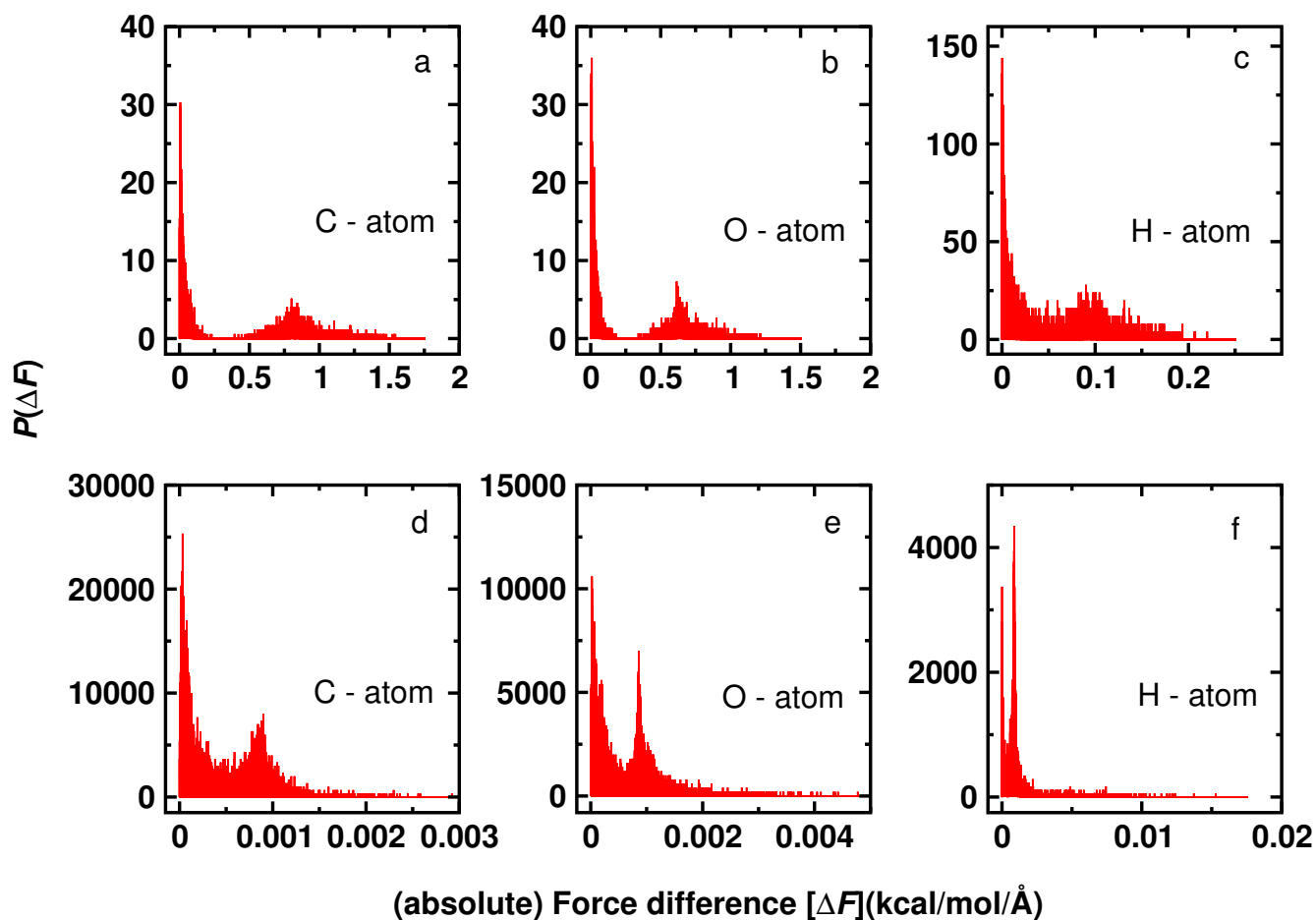


Figure S2: The probability distributions of (absolute) differences in force between the MP2 forces, acting on all the components of Carbon, Oxygen and one Hydrogen atom of the H_2CO molecule calculated at 3601 geometries with three (10^{-4} , 10^{-6} and 10^{-8}) different convergence limits in the SCF. The results of 10^{-4} and 10^{-8} convergence limits are shown in panels a-c, whereas, panels d-f show the results for 10^{-6} and 10^{-8} convergence limits.

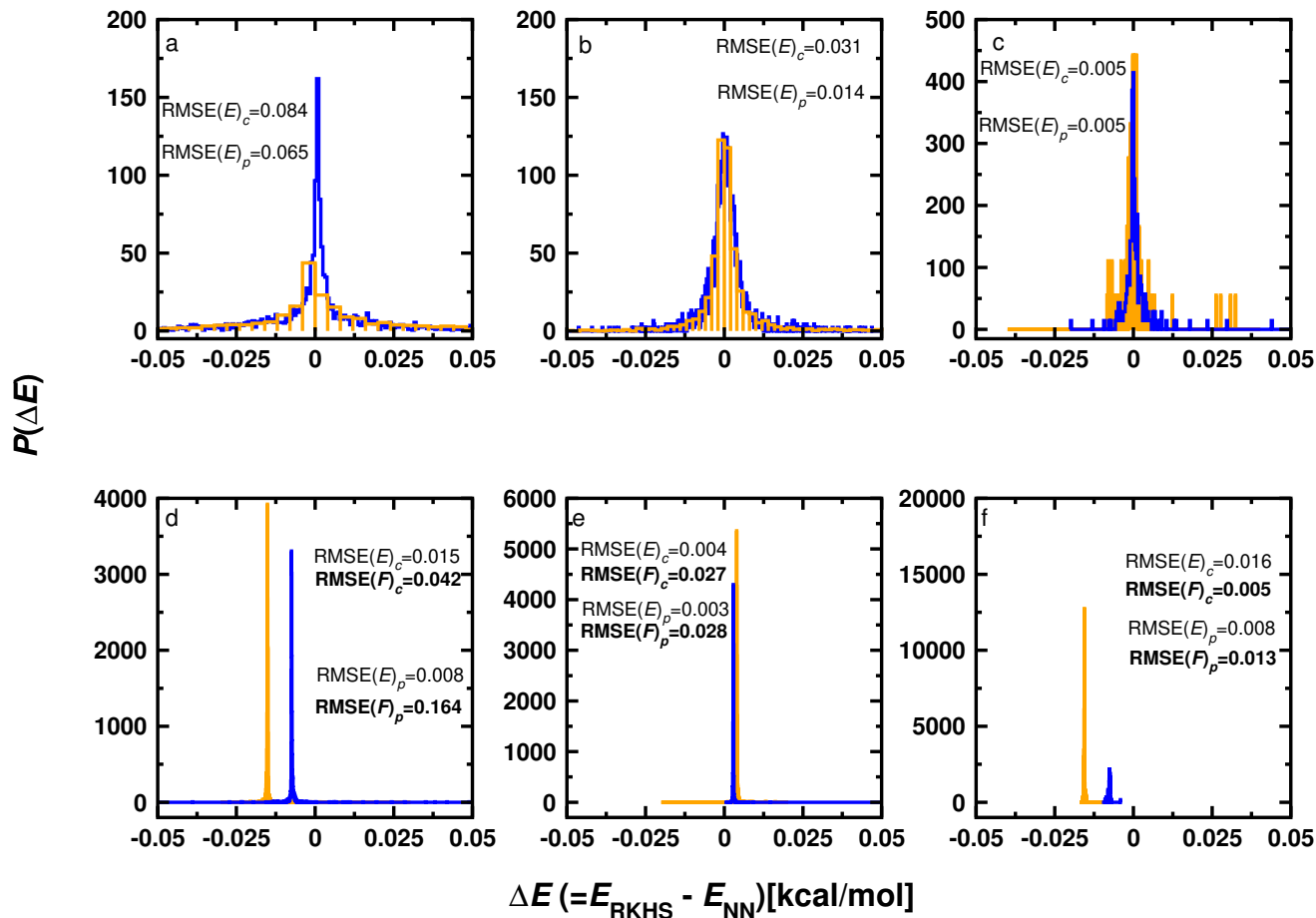


Figure S3: The probability distribution of the energy difference, $\Delta E = E_{\text{RKHS}} - E_{\text{NN}}$ for the test set for training set sizes of 500 (a, d), 1500 (b, e), and 3000 (c, f). Panels a to c: for “energy-only” training; panels d to f: for energy+force training. Clean (orange) energies and forces correspond to the RKHS energies and forces for H₂CO whereas the perturbed (blue) datasets refer to the sets obtained by adding random Gaussian noise with $\text{SD} = 10^{-6}$ eV (2.31×10^{-5} kcal/mol) on energies and $\text{SD} = 10^{-6}$ eV/Å (2.31×10^{-5} kcal/mol/Å) on forces. For each dataset size, the data corresponds to the best of the two training calculations. $\text{RMSE}(E)_c$ and $\text{RMSE}(E)_p$ represent the root-mean square error value in energy for the clean and ‘noisy’ datasets, respectively. $\text{RMSE}(F)_c$ and $\text{RMSE}(F)_p$ also have the same meaning but for the forces.

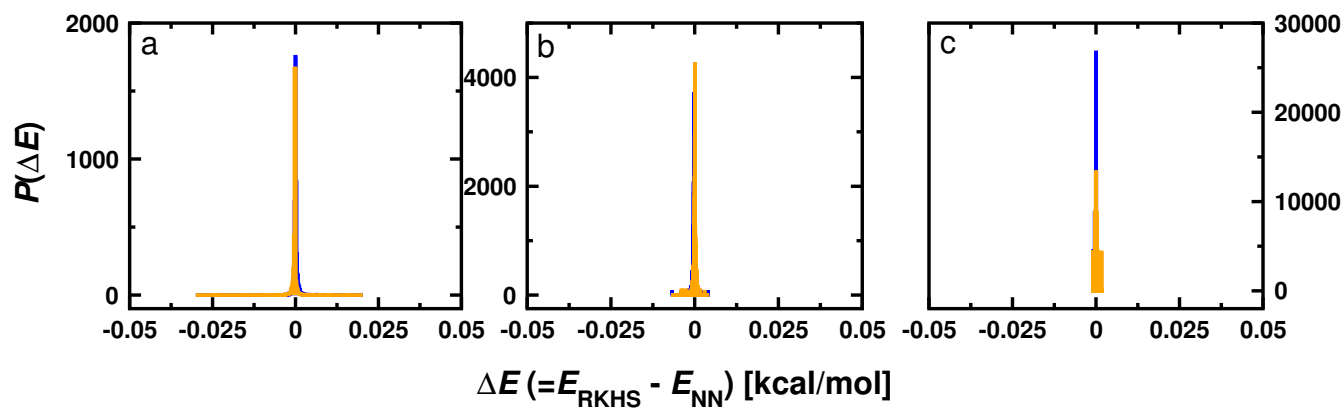


Figure S4: The probability distribution of the energy difference, $\Delta E = E_{\text{RKHS}} - E_{\text{NN}}$, for the H_2CO test set for training set sizes of 500 (a), 1500 (b) and 3000 (c). The trainings are for clean energy with clean force (orange) and clean energy with noisy ($\text{SD} = 10^{-5} \text{ eV/\AA}$) force data (blue) and with force weighting hyperparameter, $w_{\text{F}} = 1$. For training with $w_{\text{F}} \sim 53$ see Figure 5d to f.

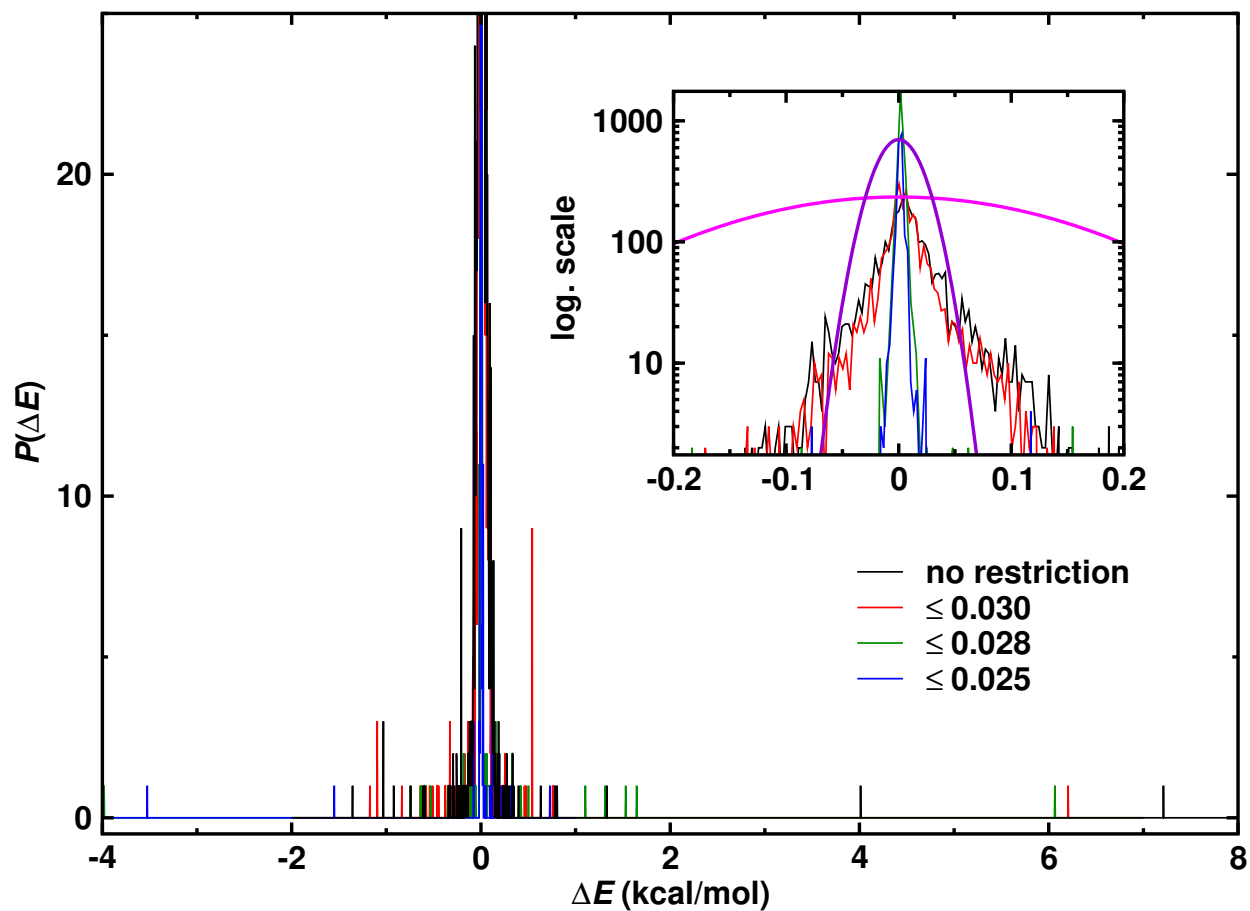


Figure S5: The probability distribution of prediction errors $P(\Delta E)$ for HONO trained on MP2 energies depending on the T_1 amplitude, see Figure 8. The inset shows a close-up of the main figure and for the data without restriction (black) and ≤ 0.025 (blue) on the T_1 amplitude Gaussians (magenta and violet, respectively) centered around $\Delta E = 0$ show the asymmetric distribution of the error towards $\Delta E > 0$.

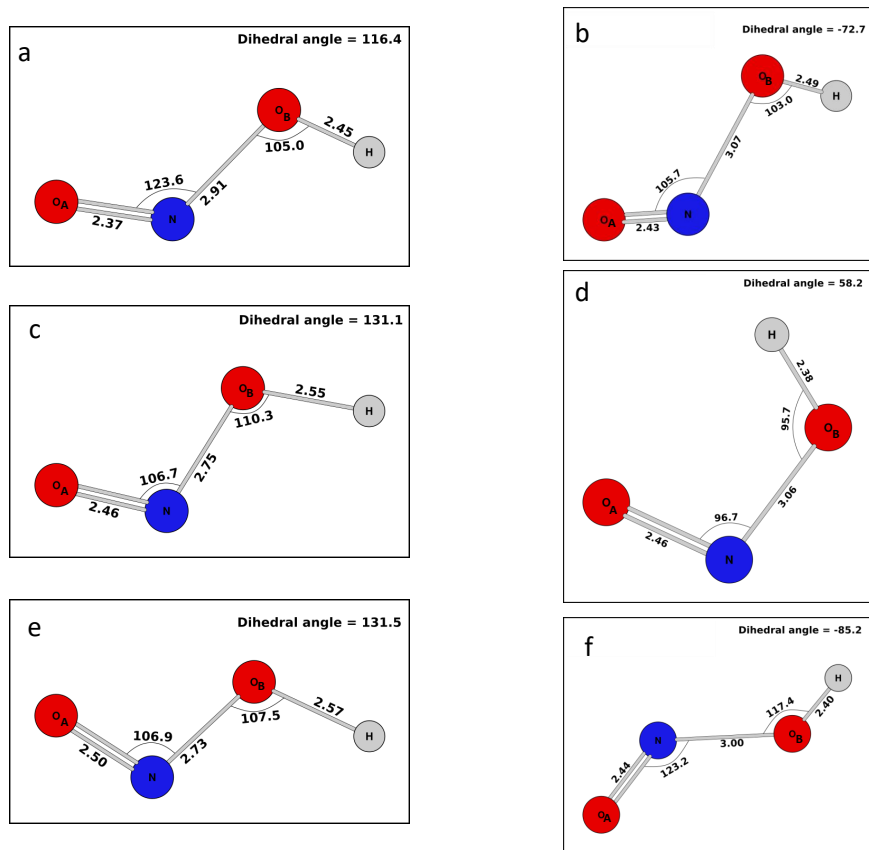


Figure S6: Structures for HONO encircled in Figure 10b. The optimized(MP2/aug-cc-pVTZ)/equilibrium structure of *trans*-HONO has $R_{O_B H} = 1.83a_0$, $R_{O_B N} = 2.70a_0$, $R_{N O_A} = 2.22a_0$, $\theta_{H O_B N} = 101.6^\circ$, and $\theta_{O_A N O_B} = 110.7^\circ$ and 180.0° dihedral angle. The six structures displayed are distorted significantly away from the minimum energy structure. Apart from the dihedral angle, the distortion takes place due to elongation of bonds and closing/opening up valence angles. For example, the structure in panel a has noticeably longer $R_{O_B H}$ bond length and widely open $\theta_{O_A N O_B}$. Furthermore, the structure in panel b has longer bond lengths for all three bonds, whereas the structure with 58.2° dihedral angle has a narrow $\theta_{O_A N O_B}$ angle.

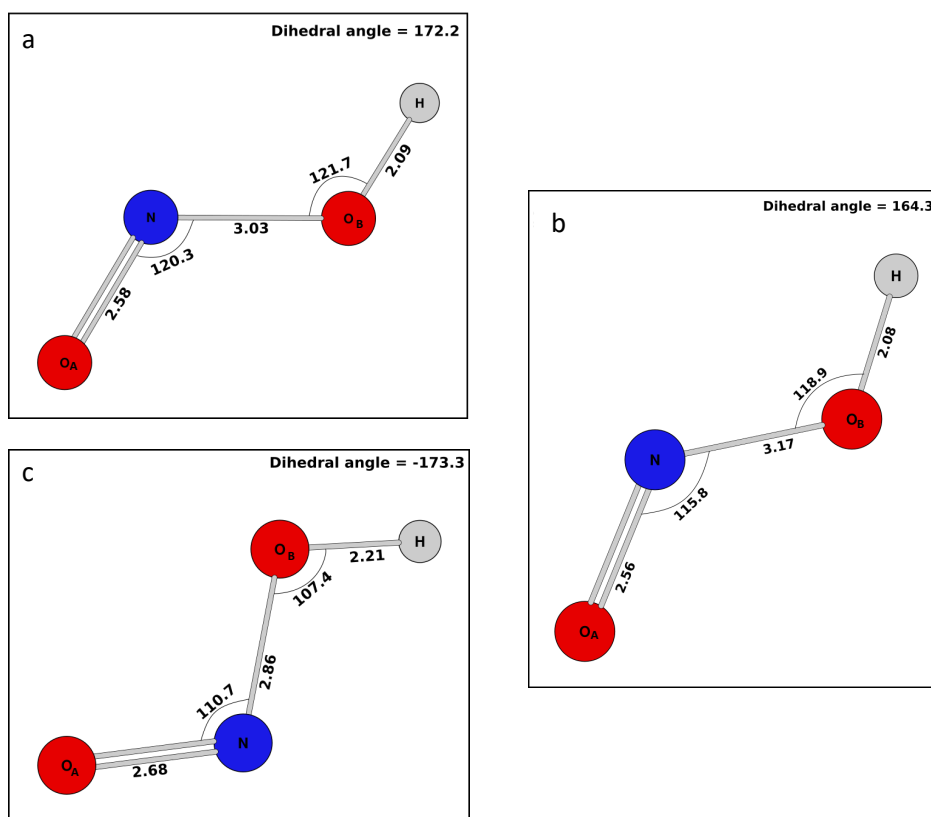


Figure S7: As Figure S6 but for structures encircled in Figure 10a. Unlike the structures shown in Figure S6, the dihedral angles are close to the optimized/equilibrium structure of *trans*-HONO. The noticeable distortion occurs for these three structures due to longer bond lengths and opening up of bond angles. For example, both bond angles are wider for the structure shown in panel a. The structure of panel b has longer R_{NO_A} bond length and wider $\theta_{\text{HO}_B\text{N}}$ bond angle.